

# POLITECNICO DI TORINO

Master's Degree in Mechatronic Engineering



Master's Degree Thesis

## Micro-slip control of automated manual transmission system through Hybrid Model Predictive Control methodologies

Supervisors

Prof. Massimo CANALE

Prof. Vito CERONE

Prof. Diego REGRUTO TOMALINO

Candidate

Marco BENINTENDE

April 2021



## Abstract

The increasing needs of car drivers in terms of fuel economy and comfort have pushed the automotive industries towards the development of innovative transmission systems and control methods to guarantee better performance and high efficiency in modern vehicles.

A suitable transmission of the internal combustion engine torque, which is non-uniform and oscillatory by its nature, is crucial in this perspective, since it can lead to high mechanical stress on driveline components and unpleasant feeling on car passengers.

Micro-slip control approach for Automated Manual Transmission (AMT) is a well affirmed technique among car manufactures thanks to its effectiveness in the attenuation of vibrations and smooth shifting. In particular, the micro-slip strategy aims at controlling the transmitted torque to avoid the complete engagement of the clutch by regulating the relative speed between the clutch discs.

In this context, a problem of paramount importance is the sign inversion of the clutch relative speed that occurs when sudden acceleration/deceleration maneuvers are performed. In such a situation, the dynamical model of the transmission changes making challenging the design of the micro-slip controller.

In the present thesis, developed in collaboration with Centro Ricerche Fiat (CRF), an original approach to micro-slip control based on Model Predictive Control methodologies is introduced aimed at attenuating the torsional oscillation in the transmission driveline and accounting for the sign inversion in the clutch relative speed.

The first contribution of the thesis is the development of a suitable Piecewise Affine (PWA) model of the transmission system that explicitly describes the sign inversion phenomenon of the clutch relative speed. The next contribution is the introduction of an original formulation of the micro-slip control problem in the framework of a Hybrid Model Predictive Control (HMPC) that can effectively handle the design problem in the presence of the considered PWA model. Finally, extensive simulation tests performed on a realistic non-linear transmission model are introduced to show the effectiveness of the proposed approach.

# Acknowledgements

*First of all, I would like to express my deepest appreciation to my supervisor Massimo Canale for all the support and encouragement he gave me during the coronavirus pandemic period. Without his wise guidance and constant feedback this thesis project would not have been achievable.*

*I would like also to thank Centro Ricerche Fiat and the System Identification & Control research group for having provided me the chance to take part in this interesting field of study. This opportunity has meant to me a moment of personal and professional growth.*

*A special dedication to my parents, whose love and constant support have let me to continue my studies with passion and serenity. I devote all my work to them. To my sister Daniela, who has always shared my sacrifices and successes despite the distance.*

*This journey would not have been possible without my Giulia. Thank you for taking care of me as you do every day even in the most difficult moments of my life. Your love makes this achievement even more valuable.*

*Last but not least, to my friends and roommates, thank you for listening, offering me advice and supporting me through this entire process. It is a real fortune to always have you next to me.*



# Table of Contents

<b>List of Tables</b>	VI
<b>List of Figures</b>	VII
<b>Acronyms</b>	XI
<b>1 Introduction</b>	1
<b>2 Overview of Dual Clutch Transmission system</b>	4
2.1 C635 DDCT Transmission . . . . .	4
2.2 Dry Dual Clutch Unit . . . . .	6
2.3 Electro-hydraulic actuation system . . . . .	6
2.4 C635 DDCT control unit . . . . .	8
<b>3 Transmission model and micro-slip control</b>	10
3.1 Driveline linear model . . . . .	10
3.2 Actuator model . . . . .	13
3.3 Micro-slip approach . . . . .	14
3.4 State of Art . . . . .	15
3.4.1 Slipping speed inversion problem . . . . .	17
<b>4 Hybrid systems and Optimal Control formulation</b>	20
4.1 Hybrid models . . . . .	20
4.1.1 Discrete Hybrid Automata . . . . .	20
4.1.2 Piecewise Affine systems . . . . .	21
4.1.2.1 Driveline PWA model . . . . .	22
4.1.3 Mixed Logical Dynamical systems . . . . .	23
4.2 The HYSDEL modeling language . . . . .	24
4.3 Model Predictive Control of Hybrid systems . . . . .	25
4.3.1 Overview of MPC technique . . . . .	25
4.3.1.1 Predictive model . . . . .	26

4.3.1.2	Cost function and optimization problem . . . . .	27
4.3.1.3	The Receding Horizon principle . . . . .	29
4.3.2	MPC for hybrid MLD systems . . . . .	30
4.3.3	Actuator delay effects . . . . .	31
4.3.4	Tracking problem . . . . .	32
4.3.5	Integral action . . . . .	32
<b>5</b>	<b>Micro-slip control system design</b>	<b>34</b>
5.1	Engine . . . . .	35
5.2	Load effects . . . . .	35
5.3	Actuator block . . . . .	36
5.4	Reference Generator . . . . .	37
5.5	Hybrid MPC design . . . . .	39
5.5.1	Transmission predictive model . . . . .	39
5.5.2	Cut-off logic . . . . .	43
5.5.3	Transmission cost function and optimization . . . . .	44
5.5.4	Hybrid Kalman filter . . . . .	46
<b>6</b>	<b>Simulation results</b>	<b>49</b>
6.1	Tests without state observer . . . . .	49
6.2	Tests with hybrid Kalman filter . . . . .	56
6.2.1	Transmissibility coefficient variation . . . . .	60
6.3	Observations . . . . .	65
<b>7</b>	<b>Conclusions</b>	<b>69</b>
7.1	Future works . . . . .	70
	<b>Bibliography</b>	<b>71</b>

# List of Tables

3.1	DDCT main parameters. . . . .	12
4.1	Basic conversion of Boolean relations into mixed-integer inequalities, with $\delta \in \{0,1\}$ . Relations involving the inverted literals $\sim \delta$ can be obtained by substituting $(1-\delta)$ for $\delta$ in the corresponding inequalities. More conversions are reported in [10]. . . . .	24
6.1	Hybrid MPC design parameters. . . . .	50

# List of Figures

2.1	C635 Fiat Power-train Technologies transmissions. Left panel MT, right panel DDCT counterpart. . . . .	4
2.2	C635 DDCT cross section. Odd-gear clutch K1 in red, even-gear clutch K2 in blue. . . . .	5
2.3	DCT configuration on left panel. Scheme of K1 and K2 clutches on right panel. . . . .	6
2.4	<b>(a)</b> Hydraulic Power Unit (PU), <b>(b)</b> complete Clutch and gear Actuation Module (CAM). . . . .	7
2.5	Complete Actuation System (CAS) hydraulic circuit. . . . .	8
3.1	One-clutch driveline scheme. . . . .	11
3.2	Driveline simplified model. . . . .	11
3.3	Single clutch model schematic. . . . .	13
3.4	Controlled actuator structure. The feedback control system assures the tracking of a suitable reference signal $x_p^{req}$ computed through the inversion of the map (3.5). While $C_f^{req}$ is the requested clutch torque, $C_f$ is the actual actuated torque. . . . .	14
3.5	Decoupling control system scheme presented in [2]. . . . .	16
3.6	General closed-loop scheme during the slipping-closing phase in [3].	16
3.7	schematic of the MPC controller from [6]. . . . .	17
3.8	Schematic from [7]: micro-slip control of a DDCT system using MPC methodologies. . . . .	18
4.1	A Discrete Hybrid Automaton (DHA) is the connection of a Finite State Machine (FSM) and a Switch Affine System (SAS), through a Mode Selector (MS) and an Event Generator (EG). . . . .	21
4.2	Piecewise Affine (PWA) systems. Mode switches are only triggered by linear threshold events [9]. . . . .	22
4.3	Basic structure of Model Predictive Control. . . . .	26
4.4	The RH controller $\mathcal{K}(\cdot)$ as the solution of QP. . . . .	30

5.1	Micro-slip control architecture. The detailed non-linear transmission system outputs the only measurable velocities $\omega_m, \omega_p$ and $\omega_r$ . . . . .	34
5.2	Engine torque profiles for first and third gear. Panel <b>(a)</b> : $C_m$ torques with partial release of the acceleration pedal. Panel <b>(b)</b> : $C_m$ torques with complete release of the acceleration pedal. . . . .	36
5.3	Actuator block with $Cf\_req$ as input and $Cf$ as output. . . . .	37
5.4	Reference Generator (RG) block. . . . .	38
5.5	Predictive model scheme. . . . .	40
5.6	State Observer scheme. . . . .	46
6.1	Slipping speed $\omega_d$ with 1st gear engaged and partial release of the accelerator. . . . .	51
6.2	Slipping speed $\omega_d$ with 1st gear engaged and full release of the accelerator. . . . .	51
6.3	Torsion speed $\omega_{sr}$ with 1st gear engaged and partial release of the accelerator. . . . .	52
6.4	Torsion speed $\omega_{sr}$ with 1st gear engaged and full release of the accelerator. . . . .	52
6.5	Longitudinal acceleration $a_x$ with 1st gear engaged and partial release of the accelerator. . . . .	53
6.6	Longitudinal acceleration $a_x$ with 1st gear engaged and full release of the accelerator. . . . .	53
6.7	Slipping speed $\omega_d$ with 3rd gear engaged and partial release of the accelerator. . . . .	54
6.8	Slipping speed $\omega_d$ with 3rd gear engaged and full release of the accelerator. . . . .	54
6.9	Torsion speed $\omega_{sr}$ with 3rd gear engaged and partial release of the accelerator. . . . .	55
6.10	Torsion speed $\omega_{sr}$ with 3rd gear engaged and full release of the accelerator. . . . .	55
6.11	Longitudinal acceleration $a_x$ with 3rd gear engaged and partial release of the accelerator. . . . .	56
6.12	Longitudinal acceleration $a_x$ with 3rd gear engaged and full release of the accelerator. . . . .	56
6.13	Torsion speed $\omega_{sr}$ comparison with and without hybrid MPC controller. A full release of the accelerator and 1st gear engaged are considered. . . . .	57
6.14	Torsion speed $\omega_{sr}$ comparison with and without hybrid MPC controller. A full release of the accelerator and 3rd gear engaged are considered. . . . .	57

6.15	Engine speed $\omega_m$ in 1st gear. Comparison between the true and the estimated quantity. . . . .	58
6.16	Primary shaft speed $\omega_p$ in 1st gear. Comparison between the true and the estimated quantity. . . . .	59
6.17	Wheel speed $\omega_m$ in 1st gear. Comparison between the true and the estimated quantity. . . . .	59
6.18	Engine speed $\omega_m$ in 3rd gear. Comparison between the true and the estimated quantity. . . . .	60
6.19	Primary shaft speed $\omega_p$ in 3rd gear. Comparison between the true and the estimated quantity. . . . .	60
6.20	Wheel speed $\omega_m$ in 3rd gear. Comparison between the true and the estimated quantity. . . . .	61
6.21	Actuated clutch torque $C_f$ in 1st gear. Comparison between the true and the estimated quantity. . . . .	61
6.22	Torsion speed $\omega_{sr}$ in 1st gear. Comparison between the true and the estimated quantity. . . . .	62
6.23	Actuated clutch torque $C_f$ in 3rd gear. Comparison between the true and the estimated quantity. . . . .	62
6.24	Torsion speed $\omega_{sr}$ in 3rd gear. Comparison between the true and the estimated quantity. . . . .	63
6.25	Slipping speed for different values of the transmissibility gain $K_t$ on 1st gear. . . . .	63
6.26	Slipping speed for different values of the transmissibility gain $K_t$ on 3rd gear. . . . .	64
6.27	Torsion speed for different values of the transmissibility gain $K_t$ on 1st gear. . . . .	64
6.28	Torsion speed for different values of the transmissibility gain $K_t$ on 3rd gear. . . . .	65
6.29	Applied torque $Cf$ for different values of the transmissibility gain $K_t$ (1st gear). . . . .	66
6.30	Requested clutch torque $Cf$ for different values of the transmissibility gain $K_t$ (1st gear). . . . .	66
6.31	Applied torque $Cf$ for different values of the transmissibility gain $K_t$ (3rd gear). . . . .	67
6.32	Requested clutch torque $Cf$ for different values of the transmissibility gain $K_t$ (3rd gear). . . . .	67



# Acronyms

**AMT**

Automated Manual Transmission

**CRF**

Centro Ricerche Fiat

**PWA**

Piecewise Affine

**HMPC**

Hybrid Model Predictive Control

**MT**

Manual Transmission

**AT**

Automatic Transmission

**CVT**

Continuously Variable Transmission

**DCT**

Dual Clutch Transmission

**WDCT**

Wet Dual Clutch Transmission

**DDCT**

Dry Dual Clutch Transmission

**ICE**

Internal Combustion Engine

**FPT**

Fiat Powertrain Technologies

**CSC**

Concentric Slave Cylinder

**PU**

Power Unit

**CAM**

Clutch and gear Actuation Module

**PPV**

Pressure Proportional Valve

**QPV**

Flow Proportional Valve

**CAS**

Complete Actuation System

**LTI**

Linear Time Invariant

**PID**

Proportional Integral Derivative

**MPC**

Model Predictive Control

**ECU**

Engine Control Unit

**DHA**

Discrete Hybrid Automaton

**SAS**

Switch Affine System

**FSM**

Finite State Machine

**EG**

Event Generator

**MS**

Mode Selector

**MLD**

Mixed Logical Dynamical

**HYSDEL**

HYbrid System DEscription Language

**RG**

Reference Generator

**RH**

Receding Horizon

**QP**

Quadratic Programming

**MIQP**

Mixed-Integer Quadratic Programming

**MIP**

Mixed-Integer Programming

**SO**

State Observer

**MPT**

Multi-Parametric Toolbox

# Chapter 1

## Introduction

Nowadays, the continuous requests by cars consumers of non-standardized products has revolutionized the automotive industries together with the advancement in production and management systems. Vehicle manufactures are facing pressing challenges to meet driver's needs with new emerging technologies. Safety, comfort, performance and efficiency are crucial requisites for a vehicle to be attractive in the market, indeed, companies have been pushed in searching for the key elements which significantly improve such features in order to enhance driving experience. In this context, the transmission systems play an important role in the upgrading process of modern commercial vehicles. Transmission system aims to transfer the torque generated from the engine to the driving wheels in a smooth and efficient fashion on the basis of the driver's will. A good transmission must guarantee, among other features, better fuel economy, greater reliability of the shifting system and high performances at the same time. Many transmission systems have been developed over the years to accomplish these conflicting requirements and to optimize the engine operating conditions. Despite some particular configurations, transmissions can be classified in five different categories listed below.

- Manual Transmission (MT) has dominated the European market for decades. With a manual transmission, the driver selects all gears manually using both a movable gear selector and a driver-operated clutch. Advantages of this configuration are a relative high efficiency, compact dimensions, low manufacturing costs and great fuel economy (although this also depends heavily on the driving style itself). The price to pay lies in the manual management of the gear shift, despite this is also a matter of taste, and the interruption of tractive power during shifting cannot be denied.
- Automatic Transmission (AT) is currently the dominant transmission in the United States. Conventional automatic transmissions generally use planetary gear sets to transfer power and multiply engine torque to the drive axle.

The biggest advantages of an automatic transmission are the ability to drive without the need for a clutch and low-wear technology, on the other hand, ATs are usually heavier, larger and more expensive than manual transmissions.

- Continuously Variable Transmission (CVT) is becoming more popular due to its simple mechanical design. A typical CVT consists of two cone-shaped pulleys and a connecting belt that are able to produce a continuous variation in the ratio of the engine input speed to the driveline output speed. Such configuration allows the engine to operate at its most efficient condition for the power level required. CVTs can be expensive to repair or replace when compared to a conventional automatic transmission and some of the common problems that owners run into include overheating, slipping, and sudden loss of acceleration.
- Automated Manual Transmission (AMT) is basically a manual transmission with either electromechanical or electrohydraulic actuators added to automate both the clutch and gear selection. In this regard, AMTs offer many advantages in terms of reduction of fuel consumption compared to MTs controlled by average drivers and improvement of driving comfort, although the traction interruption problem during gear shifting persists.
- Dual Clutch Transmission (DCT) has caught the attention of many car manufacturers over the past few years. DCTs try to overcome the torque interruption problem but, at the same time, to ensure all the benefits of the AMTs. DCT consists of two independent sub-gearboxes, one for the even gear sets and the other for odd gear sets, each one is activated by separate clutches: the engaging clutch and the disengaging clutch. A gear shift process involves the engagement of the on-coming clutch and the release of the off-going clutch to ensure shifting within a short time window of traction interruption. DCT usually offers a fully automatic mode nevertheless, it gives to the driver the chance to select gears manually. Two main types of clutches are adopted in DCTs: either two wet multi-disc clutches which are bathed in oil for cooling (WDCT), or two dry single-disc clutches (DDCT).

In addition to the mechanical architecture of car's transmission, control systems play a central role in a better management of the available hardware. Quality control policies focus on reducing vibrations and abrupt movements without compromising the shift speed and driver feels. A representative example of what has been said is the so called *micro-slip* control strategy for automated transmissions, whose main objective is to decouple the transmission line from jerks coming from the Internal Combustion Engine (ICE) in order to avoid the complete engagement (also referred to as *clutch lock-up*) and leave the clutch disks in a persistent slip condition.

A technical aspect that has to be considered explicitly from control approaches of this kind concerns the management of the phenomenon of *clutch slipping speed inversion* – i.e. the change of sign of the relative speed of the clutch plates which occurs during particular operative conditions, such as sudden acceleration and deceleration, referred to as *Tip-In* and *Tip-Out* maneuvers respectively. More precisely, the occurrence of the aforementioned phenomenon introduces a non-linear dynamics within the considered model of the transmission system which has to be properly handled by model-based controllers.

The present dissertation, developed in collaboration with Centro Ricerche Fiat (CRF), focuses on the study and simulation of a novel Hybrid micro-slip Model Predictive Controller (HMPC) for an Automated Manual Transmission system with the ultimate goal of managing the slipping speed inversion problem, minimizing the torsional oscillations inside the driveline and making the clutch slipping speed to track a proper reference signal through the transmitted clutch torque control action. In this regard, a suitable Piecewise Affine system of the driveline model is formulated on the basis of a simplified description of the clutch non-linear dynamics and it is set within an hybrid optimal control framework through the use of specific hybrid systems description tools. Furthermore, another contribution of the thesis concerns the introduction of a hybrid Kalman filter which is also formulated in PWA form compatible contextually to the hybrid formulation of the overall transmission control system. For ease of analysis, the considered AMT mathematical model is an equivalent description of a single clutch transmission of a more complex Dry Dual Clutch Transmission system designed and patented by CRF.

The thesis is organized as follows.

The second chapter briefly reviews the adopted C635 DDCT system and its components. The third chapter analyzes the mathematical description of a simple transmission system together with the micro-slip control approach and what is available in literature, followed by the investigation on the slipping speed inversion problem. In the fourth chapter, the theory behind hybrid systems is outlined and the HYSDEL hybrid model description tool will be presented. An overview on MPC techniques for hybrid systems and optimal control problem customization is conducted. The fifth chapter shows the design of the micro-slip control system for a more accurate non-linear model of the transmission system and its elements. Results obtained from tests performed on first and third gear are discussed in chapter 6 in order to show the effectiveness of the adopted control solution. The last chapter exhibits the conclusions about the obtained results and considerations about possible improvements are highlighted.

## Chapter 2

# Overview of Dual Clutch Transmission system

### 2.1 C635 DDCT Transmission

The C635 Dry Dual Clutch Transmission is a six-speed, automated manual gearbox developed by Fiat Powertrain Technologies (FPT) in Verrone, Italy plant. The transmission adopts a control system developed by Magneti Marelli and incorporates an hydraulic actuation module developed by BorgWarner (Figure 2.1).

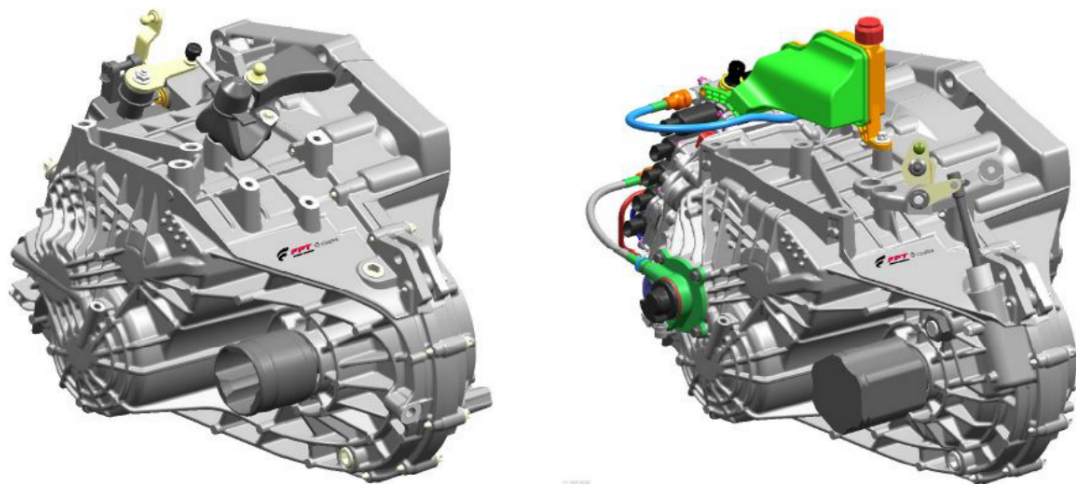


**Figure 2.1:** C635 Fiat Power-train Technologies transmissions. Left panel MT, right panel DDCT counterpart.

The C635 transmissions are transversal front wheel drive and are characterised by a three-shafts compact architecture contained in a two aluminium pieces housing with an intermediate support plate for the shaft bearings. The gear set housing is characterised by a reduced upper secondary shaft length as shown in Figure 2.2. This feature guarantees packaging in the lower segment vehicles where the longitudinal crash beam imposes serious installation constraints. The most important aspect of this transmission in terms is the adoption of a coaxial pull-rod for the actuation of the odd-gear clutch (K1), while the even-gear clutch (K2) is actuated with a rather conventional hydraulic Concentric Slave Cylinder (CSC). This pull-rod is connected to a hydraulic piston actuator located on the rear face of the transmission housing as the past one adopted in an earlier FPT technical demonstrator.

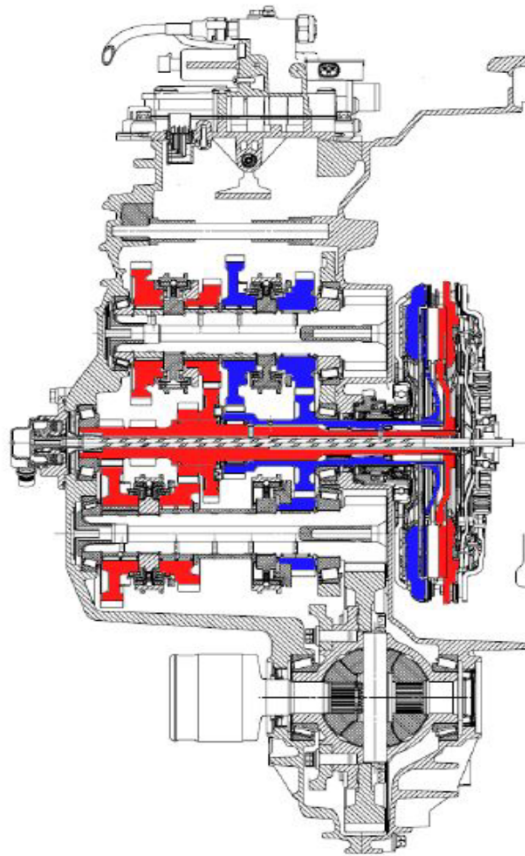


**Figure 2.2:** C635 DDCT cross section. Odd-gear clutch K1 in red, even-gear clutch K2 in blue.

## 2.2 Dry Dual Clutch Unit

The main operations and components of a DDCT are described below in order to better motivate its model decomposition into different subsystems. During the shifting process the transmitted torque is obtained through the engagement of the closing clutch and the release of the opening clutch. The K1 clutch is normally closed as in conventional manual transmissions which position is controlled by means of a contact-less linear position sensor integrated in the rear hydraulic piston actuator. The even gear K2 clutch is normally open and it is controlled in force through an hydraulic pressure given by the CSC. The two clutches act on a center plate together, thanks to their own pressure disks as shown in Figure 2.3. The entire dual clutch unit is mounted on the clutch housing by means of a single main support bearing which compact installation was developed thanks to the adoption of the specific actuation system of the K1 clutch. The dual clutch unit is linked to a dual mass flywheel mounted on the engine crankshaft through a splined connection.

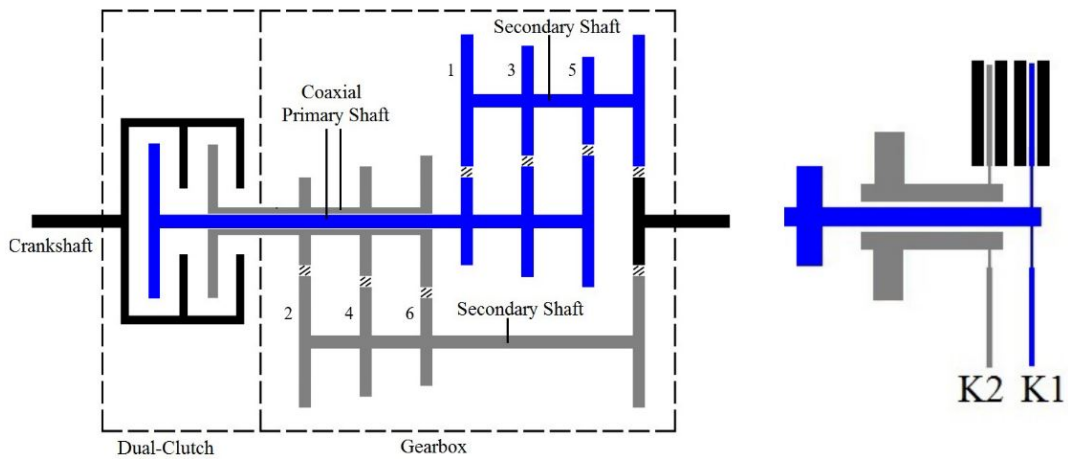


**Figure 2.3:** DCT configuration on left panel. Scheme of K1 and K2 clutches on right panel.

## 2.3 Electro-hydraulic actuation system

The C635 DDCT clutches and gear shifting mechanisms are electro-hydraulically actuated through a dedicated, sealed, hydraulic oil circuit. This choice is motivated by the compactness and overall system efficiency as well as FPT long experience with such systems among its various AMT applications. The system is composed

of an hydraulic Power Unit (PU) made up of an electrically driven high pressure pump and accumulator, depicted in Figure 2.4(a), and a Clutch and gear Actuation Module (CAM) that includes the control solenoid valves, gear shift actuators and sensors in Figure 2.4(b).

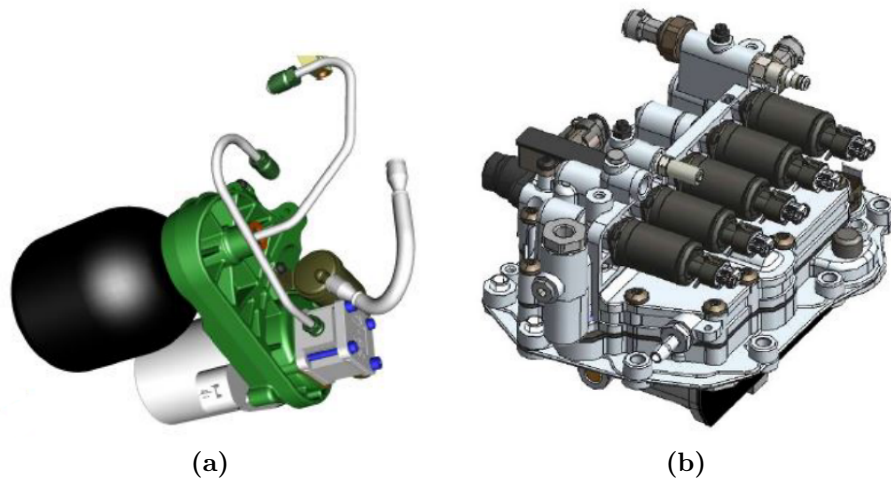


**Figure 2.4:** (a) Hydraulic Power Unit (PU), (b) complete Clutch and gear Actuation Module (CAM).

The CAM module consists of:

- four distinct double action pistons operating the gear engagement forks.
- one shifter spool which selects the piston to be actuated.
- five solenoid valves of which four are pressure proportional (PPV) and one flow proportional (QPV).

Two of the PPVs actuate the gear engagement piston which is selected by the spool valve operated by the third PPV. The fourth PPV is used for the control of the K2 clutch CSC. The QPV is used for the control of the K1 clutch position. All solenoid valves are direct derivatives of those currently used in FPT's AMT systems and, therefore, they employ well proven technology and guaranteed robustness. The actuation module also comprises five non-contact linear position sensors, one for each shifting piston and one for the spool shifter, as well as two velocity sensors reading the speed of the two primary shafts. Finally, one pressure sensor is used for the control of the K2 clutch and one for the system pressure monitoring and control. Figure 2.5 represents the hydraulic circuit of the Complete Actuation System (CAS).

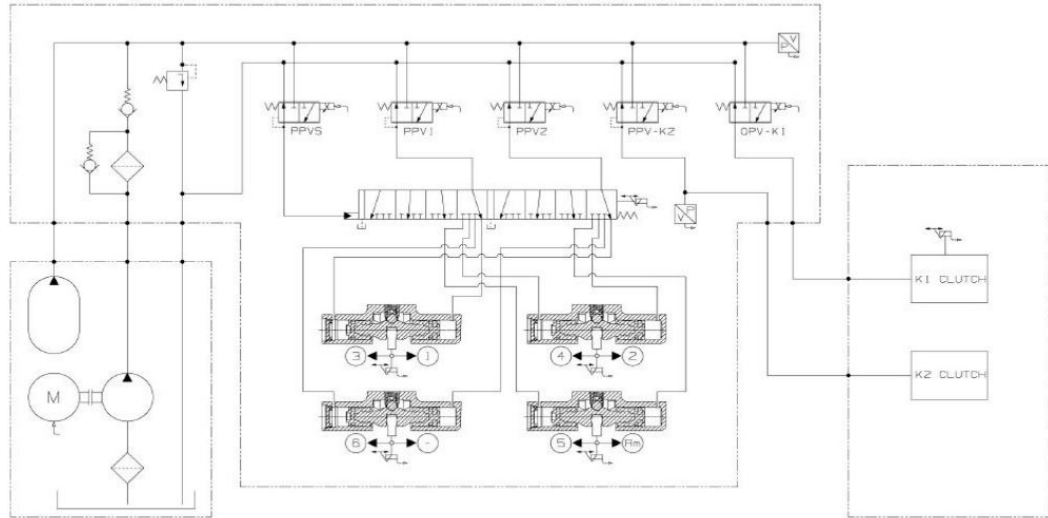


**Figure 2.5:** Complete Actuation System (CAS) hydraulic circuit.

## 2.4 C635 DDCT control unit

The C635 DDCT control strategies have been developed by FPT and run in a multitasking environment in order to meet the frequency requirements of the control loops that they implement, preserving the main micro controller resources at the same time. They can be grouped as shown below:

1. **actuator controls.** The actuator control strategies exploit the high performance attainable with electro-hydraulic actuators. The main control strategies are listed:
  - (a) engagement actuators control: based on a force/speed control concept, the desired profiles are realised by commanding the two relevant PPVs one against the other;
  - (b) shifter (selector) control: hydraulic power to the required engagement actuator is guaranteed by a fast and precise control of the shifter. The related PPV is commanded to push the shifter piston against a spring in order to reach one of the four desired positions;
  - (c) odd gears clutch controls: the normally closed clutch (K1) is controlled by a position closed loop. This is the clutch of the first and of the reverse gear; therefore, this control strategy is essential also for the vehicle starting performance;

- (d) even gears clutch: the normally open clutch (K2) is controlled in force with a pressure feedback signal delivered by one of the CAM sensors.
- 2. **Self-tuning controls.** FPT's DDC T control system has many self-tuning controls in order to compensate for the various parameters drift and to adapt the same high-level calibrations to all vehicles. The main self-tuning control algorithms concern the conversion of the requested clutch transmitted torque to K1 position and K2 pressure;
- 3. **launch and gear shift strategies.** The C635 DDC T implements various driving modes, depending on the desired performance and Brand/OEM requirements, both in manual and in automatic mode. Three different modes of shift patterns in automatic and two different ones in manual (tip) mode are contemplated. Vehicle creeping on brake release is also implemented, together with the braking systems hill holding functions.

## Chapter 3

# Transmission model and micro-slip control

A crucial aspect for the proper design of a model-based controller is the development of a mathematical description capable of capturing the most important dynamics of the transmission system. As previously discussed, a typical DDCT system consists of two distinct clutches for odd and even gear sets. Since the two clutches work using the same operating principle, a transmission system with a single clutch will be considered in order to derive a simplified linear model of both the driveline and actuator.

### 3.1 Driveline linear model

The basic components of the driveline are: the engine, the crankshaft, the clutch, the main shaft, the gearbox, the secondary shaft, the differential and the wheel shaft (see Fig. 3.1).

Three assumptions are made before formulating the equations describing the driveline dynamics:

1. Perfect rigidity of the main shaft and flexible secondary shaft;
2. Symmetry of the driveshafts;
3. Pure rolling motion of the wheels.

With the hypotheses listed above, Figure 3.2 shows the considered three masses simplified linear model of the driveline, where  $C_m$  is the engine torque,  $C_f$  is the clutch torque and  $C_{Load}$  is the load torque. Symbols  $\omega_m$ ,  $\omega_p$  and  $\omega_r$  are the angular speeds of the engine shaft, the primary shaft and the drive shaft, respectively, while

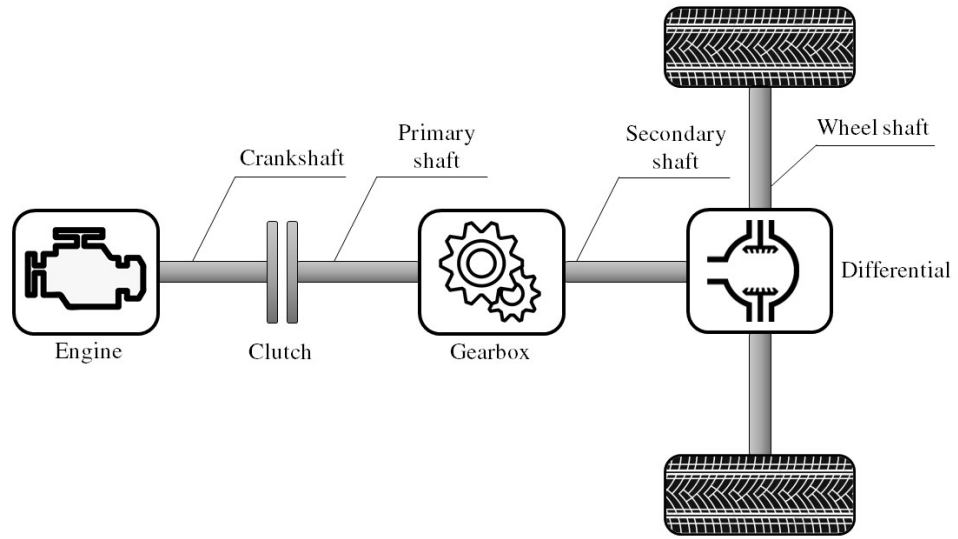


**Figure 3.1:** One-clutch driveline scheme.

the corresponding angular positions are referred as  $\theta_m$ ,  $\theta_p$  and  $\theta_r$ . Parameter values are listed in Table 3.1.

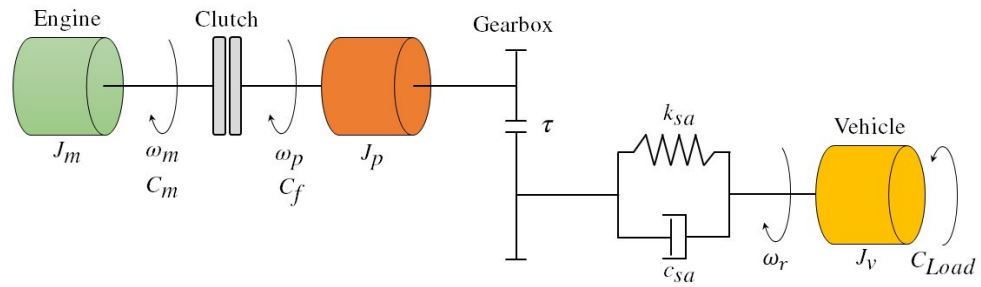


**Figure 3.2:** Driveline simplified model.

**Table 3.1:** DDCT main parameters.

Parameter	Symbol	Value	Unit
Torsional damping coefficient	$c_{sa}$	105	$Nm \cdot s/rad$
Torsional stiffness coefficient	$k_{sa}$	6719	$Nm/rad$
1st gear ratio	$\tau$	18.433	–
Wheel radius	$r_W$	0.337	$m$
Wheel inertia	$J_W$	3	$Kg \cdot m^2$
Vehicle mass	$M$	1550	$Kg$
Vehicle inertia	$J_v$	179.032	$Kg \cdot m^2$
Motor damping coefficient	$c_m$	0.019	$Nm \cdot s/rad$
Motor inertia	$J_m$	0.24	$Kg \cdot m^2$

Introducing the torsion angular position  $\theta_{sr}$  and corresponding speed  $\omega_{sr}$  as:

$$\begin{aligned}\theta_{sr} &= \frac{\theta_p}{\tau} - \theta_r \\ \omega_{sr} &= \dot{\theta}_{sr}\end{aligned}\tag{3.1}$$

by applying the second law of dynamics and imposing the rotational equilibrium for the system in Figure 3.2, the equations of the linear model are obtained:

$$\begin{aligned}J_m \dot{\omega}_m &= C_m - c_m \omega_m - C_f \\ J_p \dot{\omega}_p &= C_f + \frac{1}{\tau} [-c_{sa} \omega_{sr} - k_{sa} \theta_{sr}] \\ J_v \dot{\omega}_r &= c_{sa} \omega_{sr} + k_{sa} \theta_{sr} - C_{Load} \\ \dot{\theta}_{sr} &= \frac{\omega_p}{\tau} - \omega_r\end{aligned}\tag{3.2}$$

In the differential equations described above,  $C_m$  and  $C_{Load}$  are considered as measurable input disturbances while  $C_f$  is supposed to be the unique manipulable control input. Moreover,  $\omega_m$ ,  $\omega_p$  and  $\omega_r$  are assumed to be the only measurable output variables.

In order to express equations (3.2) in a state-space representation form, it is defined that:

- the input vector is  $u(t) = [C_m(t), C_f(t), C_{Load}(t)]^T$ ;
- the state vector is  $x(t) = [\omega_m(t), \omega_p(t), \omega_r(t), \theta_{sr}(t)]^T$ ;
- the output vector is  $y(t) = [\omega_d(t), \omega_{sr}(t)]^T$ , where  $\omega_d(t) = \omega_m(t) - \omega_p(t)$  is the so called *clutch slipping speed*.

The Linear Time Invariant (LTI) system of the simplified driveline linear model is then formulated:

$$\begin{aligned} \dot{x}(t) &= Ax(t) + Bu(t) \\ y(t) &= Cx(t) \end{aligned} \quad (3.3)$$

where  $x(t) \in \mathbb{R}^4$  is the state vector,  $u(t) \in \mathbb{R}^3$  is the system input and  $y(t) \in \mathbb{R}^2$  is the system output. With:

$$\begin{aligned} A &= \begin{bmatrix} -\frac{c_m}{J_m} & 0 & 0 & 0 \\ 0 & -\frac{c_{sa}}{J_p \tau^2} & \frac{c_{sa}}{J_p \tau} & -\frac{k_{sa}}{J_p \tau} \\ 0 & \frac{c_{sa}}{J_v \tau} & -\frac{c_{sa}}{J_v} & \frac{k_{sa}}{J_v} \\ 0 & \frac{1}{\tau} & -1 & 0 \end{bmatrix} & B &= \begin{bmatrix} \frac{1}{J_m} & -\frac{1}{J_m} & 0 \\ 0 & \frac{1}{J_p} & 0 \\ 0 & 0 & -\frac{1}{J_v} \\ 0 & 0 & 0 \end{bmatrix} \\ C &= \begin{bmatrix} 1 & -1 & 0 & 0 \\ 0 & \frac{1}{\tau} & -1 & 0 \end{bmatrix} \end{aligned} \quad (3.4)$$

## 3.2 Actuator model

The actuator allows the transmission of the clutch torque to the drivetrain. For each clutch of the DDCCT system the center plate has two contact surfaces, therefore, for the adopted single clutch model, in place of two pairs of sliding surfaces it will be considered an equivalent single pair as shown in Figure 3.3.

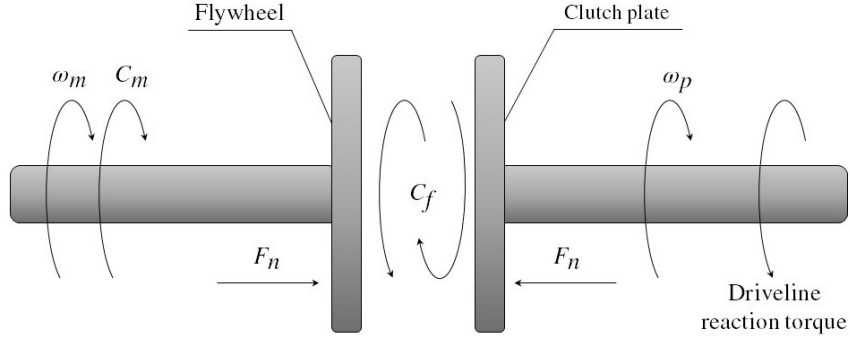


**Figure 3.3:** Single clutch model schematic.

The clutch actuator presses the clutch disks against each other. The friction due to their contact allows the transmission of the clutch torque which can be controlled by varying the clamping normal force  $F_n$ . In the present study, the existence of a feedback controlled clutch actuator is assumed to improve the actuation accuracy

performance (see Fig. 3.4). More precisely, the controlled actuator is responsible of generating the clutch torque on the basis of the one requested by the high-level micro-slip controller through the adoption of a static map which describes the relationship between  $C_f$  and the clutch throw-out bearing position  $x_p$  as follows:

$$C_f = \mathcal{M}(x_p) \quad (3.5)$$



**Figure 3.4:** Controlled actuator structure. The feedback control system assures the tracking of a suitable reference signal  $x_p^{req}$  computed through the inversion of the map (3.5). While  $C_f^{req}$  is the requested clutch torque,  $C_f$  is the actual actuated torque.

As far as the first consideration is concerned, the actuator structure depicted in Figure 3.4 can be approximated by a second order transfer function with  $C_f^{req}$  as input and  $C_f$  as output of the form:

$$G_{act}(s) = \frac{C_f(s)}{C_f^{req}(s)} = K_t \frac{\omega_n^2}{s^2 + 2\xi\omega_n s + \omega_n^2} e^{-\theta s} \quad (3.6)$$

In the model (3.6),  $K_t$  is the clutch transmissibility gain which accounts for the torque map characteristics,  $\theta$  is the overall actuation delay and  $\xi$  and  $\omega_n$  are the pole damping coefficient and natural frequency respectively. The second consideration is that, variations on the clutch transmissibility characteristics due to, e.g. different temperature operating conditions, can be approximately described by a parametric uncertainty on the  $K_t$  coefficient.

### 3.3 Micro-slip approach

With reference to Figure 3.3, three different clutch operating conditions are recognized:

1. Open clutch phase: the two disks are completely disengaged so that  $C_f = 0$ ;

2. Slipping phase: if there exists a relative speed between the engine and the primary shaft – i.e. the slipping speed  $\omega_d$  differs from zero;
3. Closed clutch phase: the clutch is locked-up and the engine torque is fully transmitted to the driveline,  $C_f = C_m$ .

The micro-slip approach concerns the slipping phase.

In powertrain systems equipped with ICE, the torque transmission is decisive: due to its discontinuous and intermittent nature it often leads to a floaty behaviour of the engine shaft acceleration so that, whenever complete clutch engagement occurs, this undesired effect is transmitted to the drivetrain causing unpleasant feeling on car passengers. In addition, during sudden accelerations and decelerations, the elasticity of the mechanical elements of the driveline can lead to torsional oscillation of the shafts together with high stresses on delicate vehicle parts.

It has been experimentally proven that a controlled slight slip between the clutch disks can guarantee several advantages in terms of comfort and preservation of mechanical components [1]. Indeed, the introduction of the micro-slip control during transients, before reaching the clutch lock-up, determines a better smooth engagement reducing jerks produced by the ICE and driveline oscillations. Even letting the micro-slip replace the no-slip phase, a better working condition of the driveline is achieved due to the almost complete decoupling of the drivetrain from the high frequency dynamics of the engine. In the latter case, the fuel consumption remains unchanged together with a full achievement of comfortable driveability at the price of an increase in wear due to the continuous friction power dissipation that can be compensated through a lubrication control action.

### 3.4 State of Art

Different control architectures have been proposed in the literature that adopts the micro-slip framework in order to reduce the transmitted torque oscillations inside a dry clutch transmission system.

In [2] a decoupled control system with two independent PID controllers tracks optimized speed references separately: the engine speed  $\omega_e$  and the clutch slipping speed. The analyzed feedback system in Figure 3.5 assures a smooth clutch engagement.

The main goal of the control system exploited in [3] is to reach the clutch lock-up quickly avoiding the engine stall. It is based on a hierarchical approach by discriminating among five different AMT operating conditions: engaged, slipping-opening, synchronization, go-to-slipping and slipping-closing. The control scheme consists of decoupled and cascaded feedback loops based on measurements of the

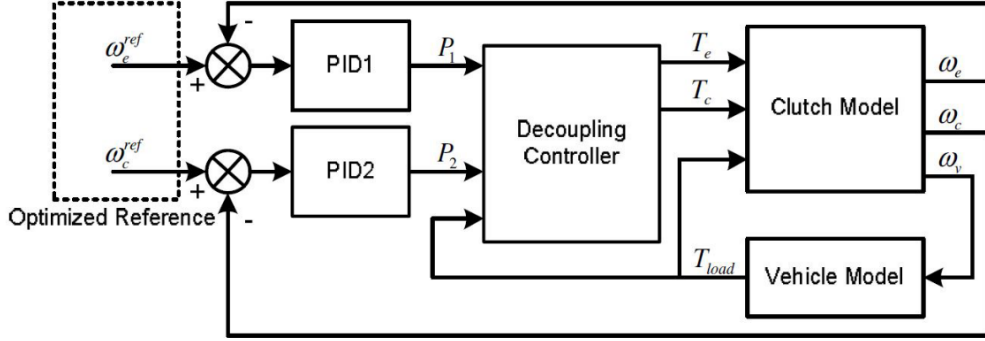


Figure 3.5: Decoupling control system scheme presented in [2].

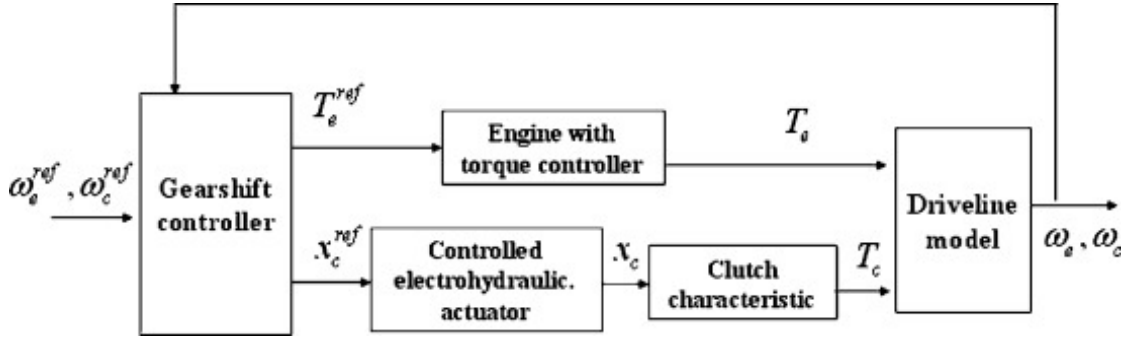


Figure 3.6: General closed-loop scheme during the slipping-closing phase in [3].

engine speed, clutch speed, and throw-out bearing position (see Fig. 3.6). The transmitted torque is estimated.

In [4] the authors present a Linear Quadratic control system that follows an optimal control approach by using the crankshaft speed and the clutch speed as state variables. The chosen control variables are the engine and the clutch torque. In this strategy, however, constraints on control input and state variables are not considered explicitly in the solution. To overcome this limitation, the same authors propose the adoption of a Model Predictive Control (MPC) methodology in [5]. The developed controller minimizes a quadratic performance index that takes into account the clutch friction losses and speed regulation, subject to constraints on control and state variables.

In [6] the introduced control system, shown in Figure 3.7, adopts the clutch

torque as the only manipulable control variable whereas, due to hard technological constraints in modern vehicles, the engine torque is treated as a known non-controllable input. In the proposed architecture the Engine Control Unit (ECU)

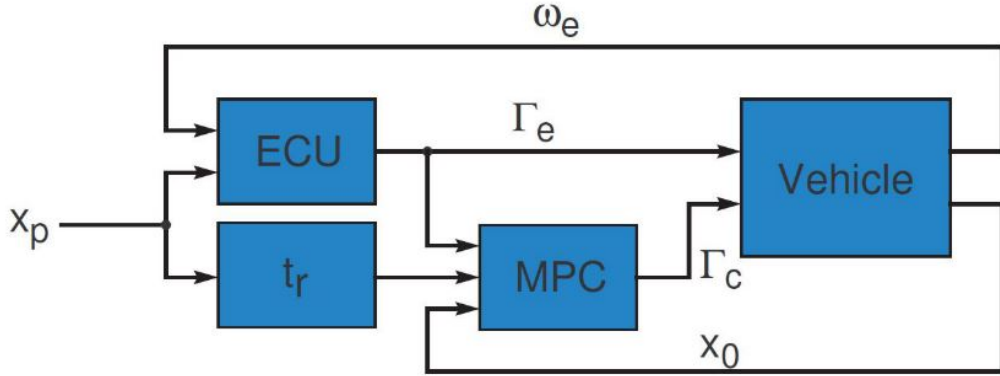


**Figure 3.7:** schematic of the MPC controller from [6].

outputs the engine torque  $\Gamma_e$  obtained on the basis of the throttle pedal position  $x_p$ . The total engagement time  $t_f$ , that is computed in function of  $x_p$ , is used to calculate the time control horizon denoted as  $t_r$ . The clutch torque is then realized through the MPC control strategy, solving the optimal control problem with a suitable cost function.

A further study conducted in [7] shows the design of an original micro-slip MPC control system whose objective is to make the clutch slipping speed tracking a suitable reference signal through the clutch torque control action, ensuring the minimization of the driveline oscillations by means of the zero regulation of the drive shaft torsion speed. Finally, the proposed control system, depicted in Figure 3.8, introduces proper constraints on the transmitted clutch torque and slipping speed. More precisely, while the clutch torque has to be positive and cannot exceed its maximum value, the clutch lock-up is avoided during the entire maneuver.

The feedback control systems described above are effective solutions to the micro-slip approach problem. Nevertheless, in the literature there are no studies about feedback MPC controllers that explicitly take into account the sign inversion of the slipping speed  $\omega_d$  and its consequences. To better understand such limitation, the slipping speed inversion phenomenon is investigated in the next section.

### 3.4.1 Slipping speed inversion problem

As previously discussed, during some particular operating conditions, e.g. tip-in and tip-out maneuvers, the primary shaft speed  $\omega_p$  can rotate faster than the engine

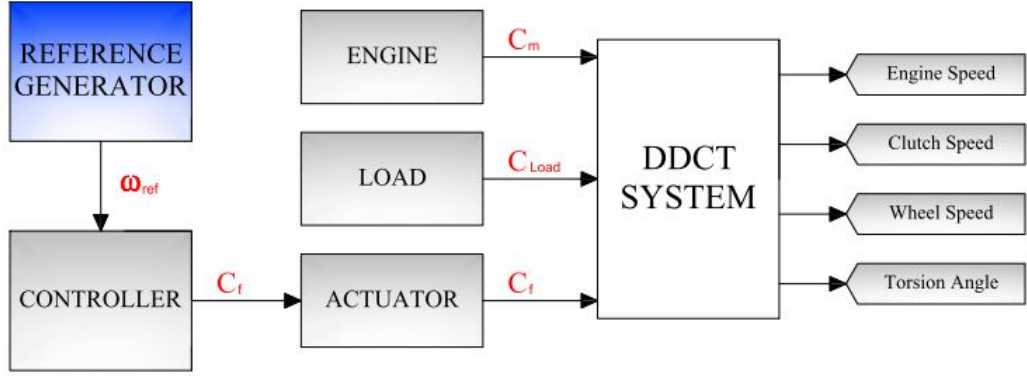


**Figure 3.8:** Schematic from [7]: micro-slip control of a DDCT system using MPC methodologies.

shaft speed  $\omega_m$  leading to the sign change of their relative velocity – i.e.  $\omega_d$ . In [8] different clutch models are proposed. As a first approximation, the most simple clutch dynamic during slipping is considered:

$$C_f = n\mu R_e F_n \text{sign}(\omega_d) \quad (3.7)$$

Where  $n$  is the number of friction surfaces,  $\mu$  the friction coefficient and  $R_e$  the effective radius of the clutch. Symbols  $C_f$  and  $F_n$  indicate the clutch torque and the clamping normal force respectively, as represented in Figure 3.3.

As it can be seen from eq. (3.7), sudden inversions of the slipping speed induce sign changes of the clutch torque. Nevertheless, due to the physical architecture of the considered actuator,  $C_f$  values can only be either positive so that the clutch torque is transmitted to the drivetrain (partially or completely), or equal to zero (the clutch torque is no more transmitted). Therefore, the driveline dynamic equations formulated in (3.2) will be necessarily subject to straightforward modifications. More precisely, assuming that parameters  $n$ ,  $\mu$ ,  $R_e$  and  $F_n$  are directly computed from the low-level controller depicted in Figure (3.4), the system presented in (3.3) will be no more time invariant but slipping speed switching dependent:

$$\begin{aligned} \dot{x}(t) &= Ax(t) + B(\omega_d(t))u(t) \\ y(t) &= Cx(t) \end{aligned} \quad (3.8)$$

with:

$$B(\omega_d(t)) = \begin{bmatrix} \frac{1}{J_m} & -\frac{1}{J_m} \text{sign}(\omega_d(t)) & 0 \\ 0 & \frac{1}{J_p} \text{sign}(\omega_d(t)) & 0 \\ 0 & 0 & -\frac{1}{J_v} \\ 0 & 0 & 0 \end{bmatrix} \quad (3.9)$$

Due to the reasons mentioned above, a proper control system has to be developed in order to be consistent with the actual driveline operating conditions – i.e. in the presence of either positive or negative slipping speed.

In the present dissertation, an extension of the work presented in [7] is proposed in order to manage the slipping speed sign inversion phenomenon through the development of a suitable Piecewise Affine (PWA) system. Such system will be taken into account in the design of a novel Hybrid MPC controller whose main goal is the tracking of a slight switching slipping speed reference and the zero regulation of the shaft torsion speed.

## Chapter 4

# Hybrid systems and Optimal Control formulation

### 4.1 Hybrid models

Hybrid systems are mathematical models whose evolution depend on a mix of real-time and discrete events. Most of the dynamical systems may reasonably be described in hybrid terms, e.g. cars, airplanes, washing machines and so on and so forth. Nevertheless, most of the literature on dynamic modeling is concerned with systems that are either completely continuous or completely discrete. Consequently, most of the control theory and tools are based on models describing the evolution of real-valued signals according to smooth linear or nonlinear state transition functions, typically differential or difference equations. In many fields, however, the system to be controlled also contains signals such as Boolean relations, if-then-else, on/off conditions which may affect real-valued signals. Hybrid systems describe in a common framework the coupling between real-valued variables and discrete variables dynamics on the basis of their interaction.

#### 4.1.1 Discrete Hybrid Automata

The Discrete Hybrid Automaton (DHA) is a modeling formalism for hybrid systems that may be thought of as an extension of finite-state machines. DHA results from the connection of a Switch Affine System (SAS), which provides the piecewise linear dynamics, with a Finite State Machine (FSM) that performs the transitions between the discrete states of the hybrid system. Such transitions are based on two connecting elements: the Event Generator (EG) and Mode Selector (MS), as shown

in Figure 4.1. The EG extracts logic signals from the continuous part and those logic events trigger the states transition in the FSM. The MS combines all the logic variables – i.e. states, inputs and events, in order to choose the SAS current continuous dynamics, also referred as *mode*. Further details on DHA components are presented in [9]. DHA generalizes many models oriented to computational tools for hybrid systems and therefore it represents the starting point for the solution of complex analysis and synthesis problems of hybrid systems. However DHA is difficult for analysis and control because the verification and simulation procedures are computationally hard.

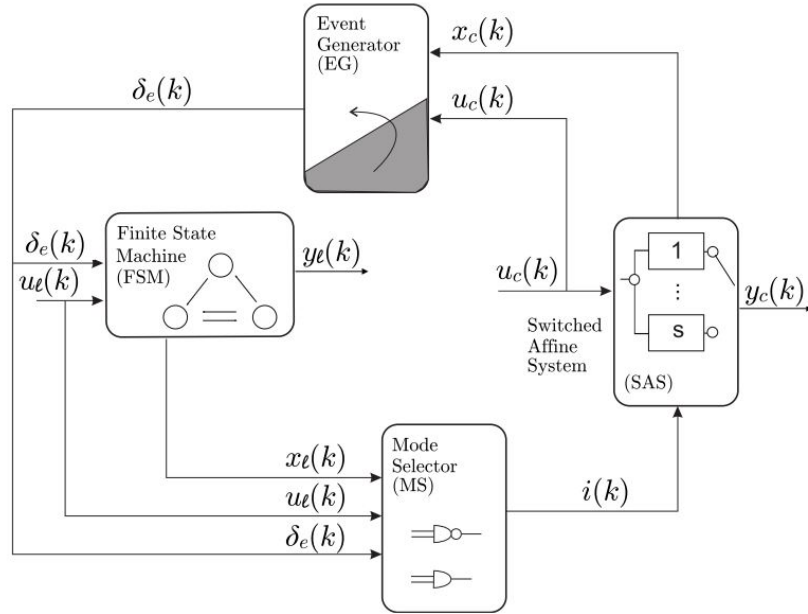


**Figure 4.1:** A Discrete Hybrid Automaton (DHA) is the connection of a Finite State Machine (FSM) and a Switched Affine System (SAS), through a Mode Selector (MS) and an Event Generator (EG).

### 4.1.2 Piecewise Affine systems

A particular case of DHA is the popular class of Piecewise Affine (PWA) systems. Essentially, they are switched affine systems whose mode depends on the current location of the state vector, as depicted in Figure 4.2. More precisely, PWA systems are defined by partitioning the space of states and inputs into polyhedral regions and associating within each region different affine state-update and output equations as follows:

$$x(k+1) = A^{i(k)}x(k) + B^{i(k)}u(k) + f^{i(k)}, \quad (4.1a)$$

$$y(k) = C^{i(k)}x(k) + D^{i(k)}u(k) + g^{i(k)}, \quad (4.1b)$$

$$i(k) \text{ such that: } H^{i(k)}x(k) + J^{i(k)}u(k) \leq K^{i(k)}, \quad (4.1c)$$

where  $x(k) \in \mathbb{R}^n$  is the state vector at time  $k \in \mathbb{K}$  and  $\mathbb{K} \triangleq \{0, 1, \dots\}$  is the set of non-negative integers,  $u(k) \in \mathbb{R}^m$  is the input vector,  $y(k) \in \mathbb{R}^p$  is the output vector,  $i(k) \in \mathcal{I} \triangleq \{1, \dots, s\}$  establishes the current mode of the system and matrices  $A^{i(k)}$ ,  $B^{i(k)}$ ,  $f^{i(k)}$ ,  $C^{i(k)}$ ,  $D^{i(k)}$ ,  $g^{i(k)}$ ,  $H^{i(k)}$ ,  $J^{i(k)}$ ,  $K^{i(k)}$  are constant and have suitable dimensions. The inequalities in (4.1c) should be interpreted component-wise and each of them defines a half-space in  $\mathbb{R}^n$  and a corresponding hyperplane that is referred to as *guardline*. Each vector inequality (4.1c) defines a polyhedron  $\mathcal{C}^i = \left\{ \begin{bmatrix} x \\ u \end{bmatrix} \in \mathbb{R}^{n+m} : H^i x + J^i u \leq K^i \right\}$  in the state+input space  $\mathbb{R}^{n+m}$ .

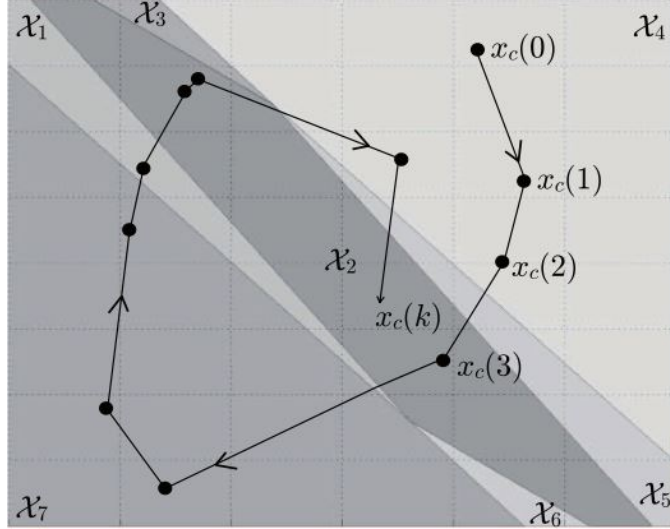


**Figure 4.2:** Piecewise Affine (PWA) systems. Mode switches are only triggered by linear threshold events [9].

#### 4.1.2.1 Driveline PWA model

Before introducing the driveline PWA model description, a discretization of the continuous-time dynamic driveline system is performed:

$$\begin{aligned} x_{cd}(k+1) &= A_{cd}x_{cd}(k) + B_{cd}u_{cd}(k) \\ y_{cd}(k) &= C_{cd}x_{cd}(k) \end{aligned} \quad (4.2)$$

where:

- $x_{cd}(k) = [\omega_m(k), \omega_p(k), \omega_r(k), \theta_{sr}(k)]^T$  is the driveline discrete-time state vector;
- $u_{cd}(k)$  is the model input;
- $y_{cd}(k) = [\omega_d(k), \omega_{sr}(k)]^T$  is the system output;
- $A_{cd}$ ,  $B_{cd}$  and  $C_{cd}$  result from the conversion of the state-space representation (3.3) from continuous to discrete-time.

Following the model description presented in the previous section, it is possible to recast (4.2) equations in PWA form:

$$\begin{cases} x_{cd}(k+1) = A_{cd}x_{cd}(k) + [B_{cd}(i,1) & \alpha(k)B_{cd}(i,2) & B_{cd}(i,3)] u_{cd}(k), i = 1, \dots, 4 \\ y_{cd}(k) = C_{cd}x_{cd}(k) \\ \alpha(k) = \begin{cases} 1 & \text{if } [1 \ -1 \ 0 \ 0] x_{cd}(k) \geq 0, & \text{Mode 1} \\ -1 & \text{if } [1 \ -1 \ 0 \ 0] x_{cd}(k) < 0, & \text{Mode 2} \end{cases} \end{cases} \quad (4.3)$$

where the variable  $\alpha(k)$  discriminates between the positive (Mode 1) and negative (Mode 2) slipping speed. Note that, the introduction of the two modes induces a discontinuity inside the discrete driveline dynamics which has to be treated in a proper way during simulations in order to avoid technical problems. The solution to these problems is addressed in section (5.5.2).

### 4.1.3 Mixed Logical Dynamical systems

An equivalent representation of DHA and PWA systems is the Mixed Logical Dynamical (MLD) system that is more suitable for solving optimization problems. In this perspective, it is worth saying that Boolean formulas describing the switching dynamics of the system can be equivalently represented as integer linear inequalities as reported in Table 4.1.

MLD models consist of a collection of linear difference equations involving both real and binary variables and a set of linear inequality constraints as described by the following relations:

$$x(k+1) = Ax(k) + B_1u(k) + B_2\delta(k) + B_3z(k) + B_5, \quad (4.4a)$$

$$y(k) = Cx(k) + D_1u(k) + D_2\delta(k) + D_3z(k) + D_5, \quad (4.4b)$$

$$E_2\delta(k) + E_3z(k) \leq E_1u(k) + E_4x(k) + E_5, \quad (4.4c)$$

**Table 4.1:** Basic conversion of Boolean relations into mixed-integer inequalities, with  $\delta \in \{0,1\}$ . Relations involving the inverted literals  $\sim \delta$  can be obtained by substituting  $(1 - \delta)$  for  $\delta$  in the corresponding inequalities. More conversions are reported in [10].

Relation	Boolean	Linear constraints
<b>AND</b>	$\delta_1 \wedge \delta_2$	$\delta_1 = 1, \delta_2 = 1$ <b>or</b> $\delta_1 + \delta_2 \geq 2$
<b>OR</b>	$\delta_1 \vee \delta_2$	$\delta_1 + \delta_2 \geq 1$
<b>NOT</b>	$\sim \delta_1$	$\delta_1 = 0$
<b>XOR</b>	$\delta_1 \oplus \delta_2$	$\delta_1 + \delta_2 = 1$
<b>IMPLY</b>	$\delta_1 \rightarrow \delta_2$	$\delta_1 - \delta_2 \leq 0$
<b>IFF</b>	$\delta_1 \leftrightarrow \delta_2$	$\delta_1 - \delta_2 = 0$
<b>ASSIGNMENT</b> $\delta_3 = \delta_1 \wedge \delta_2$	$\delta_3 \leftrightarrow \delta_1 \wedge \delta_2$	$\delta_1 + (1 - \delta_3) \geq 1$ $\delta_2 + (1 - \delta_3) \geq 1$ $(1 - \delta_1) + (1 - \delta_2) + \delta_3 \geq 1$

where  $x \in \mathbb{R}^{n_c} \times \{0,1\}^{m_i}$  is a vector of continuous and binary states,  $u \in \mathbb{R}^{m_c} \times \{0,1\}^{m_i}$  are the inputs,  $y \in \mathbb{R}^{p_c} \times \{0,1\}^{p_i}$  the outputs,  $\delta \in \{0,1\}^r$  are auxiliary binary variables,  $z \in \mathbb{R}^{r_c}$  are continuous auxiliary variables and  $A, B_1, B_2, B_3, C, D_1, D_2, D_3, E_1, \dots, E_5$  are matrices of suitable dimensions. Note that the constraints (4.4c) allow one to specify additional linear constraints on continuous variables (e.g., constraints over physical variables of the system), and logical constraints over Boolean variables. The ability to include constraints, constraint prioritization, and heuristics adds to the expressiveness and generality of the MLD framework. Note also that despite the fact that the description (4.4) seems to be linear, clearly the non-linearity is concentrated in the integrality constraints over binary variables.

## 4.2 The HYSDEL modeling language

The conversion of the state machine and dynamical equations of the hybrid systems into a MLD framework requires a set of rules [11]. This task is generally long and tedious and to make it easier, a computational tool called HYbrid System DEscription Language (HYSDEL) [12] is used. The HYSDEL description of a DHA is an abstract modeling step. The associated HYSDEL compiler then translates the description into several computational models, in particular into an MLD and PWA form. The HYSDEL list is composed of two parts whose main sections, useful

for the description of the hybrid models adopted in this thesis, are outlined below:

- **INTERFACE**: this part contains the declaration of all variables (states, inputs, outputs) and parameters, so that it is possible to make the proper type checks.
- **IMPLEMENTATION**: it is composed of specialized sections where the relations among the variables are stated. These sections are described next.
  - **AUX**: it contains the declaration of the auxiliary variables used in the model;
  - **AUTOMATA**: it specifies the state transition equations of the FSM as a collection of Boolean functions;
  - **AD**: this section allows one to define Boolean variables from continuous ones, and is based exactly on the semantics of the EG described earlier;
  - **DA**: it defines continuous variables according to if-then-else conditions. This section models part of the SAS;
  - **CONTINUOUS**: it describes the linear dynamics, expressed as difference equations;
  - **MUST**: this section specifies arbitrary linear and logic constraints on continuous and Boolean variables. More generally, it allows also mixed constraints on states, inputs, and outputs;
  - **OUTPUT**: it specifies static linear and logic relations for the output vector of the hybrid model.

For further details on HYSDEL features, the reader interested in the tool will find more information on [13].

## 4.3 Model Predictive Control of Hybrid systems

### 4.3.1 Overview of MPC technique

MPC is a control approach that has spread in a wide range of applications of different engineering fields due to its effectiveness in constraints handling and high performance achievement. These capabilities rely on an explicit consideration of the system model such that it is possible to obtain a control action as a result of a constrained optimization problem. Nevertheless, since a numerical optimization problem has to be solved at every sampling time, the computational burden of model-based controllers is quite high. For this reason, originally, MPCs were mainly employed in systems characterized by slow dynamics and large computational

resources such as process industries or chemical plants. However, thanks to greater computing power, MPC techniques are applied to a multitude of fast dynamic systems like flight control and automotive applications. The term Model Predictive Control does not designate a specific control strategy but rather an ample range of control methods. In spite of everything, MPC controllers make use of: the prediction model, a suitable cost function together with constraints, and the optimizer (see Fig. 4.3).

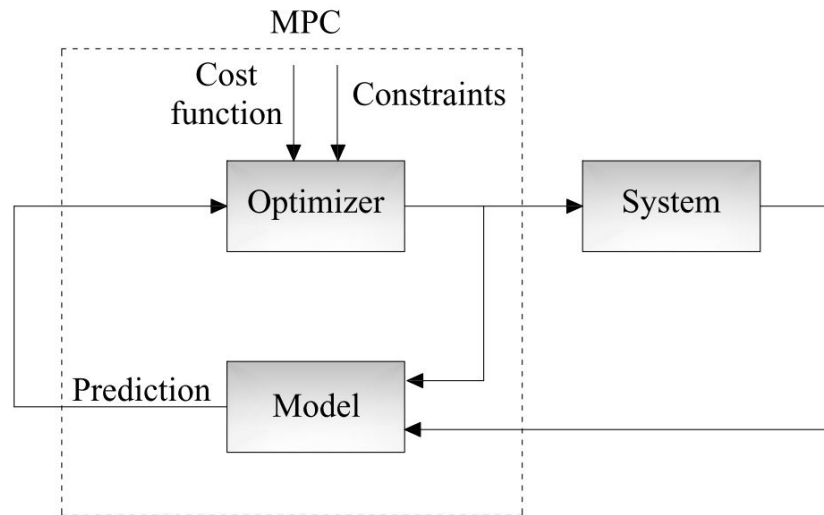


**Figure 4.3:** Basic structure of Model Predictive Control.

The main advantages of the MPC strategy can be summarized in:

1. a flexible, open and intuitive formulation in time domain;
2. the ability to manage multi-variable control problems;
3. the inclusion of both control input and state variables constraints;
4. the use of an optimal control law which results from a trade-off between different objectives, even conflicting.

#### 4.3.1.1 Predictive model

The predictive model represents a detailed description of the system to be controlled. Among the different prediction models that can be adopted, the use of a discrete

LTI system is considered:

$$\begin{aligned} x(k+1) &= Ax(k) + Bu(k) \\ y(k) &= Cx(k) \end{aligned} \quad (4.5)$$

As the name suggests, the predictive model gives the evolution of the states starting from an initial time instant  $k$  over a certain number of time steps in the future. More precisely, for a LTI system like the one in (4.5), the  $i^{\text{th}}$  step ahead state prediction  $x(k+i|k)$  is given by:

$$\begin{aligned} x(k+i|k) &= A^i x(k|k) + A^{i-1} Bu(k|k) + A^{i-2} Bu(k-1|k) + \dots + \\ &+ Bu(k+i-1|k) = A^i x(k|k) + \sum_{j=0}^{i-1} A^{i-j-1} Bu(k+j|k) \end{aligned} \quad (4.6)$$

thus,  $x(k+i|k)$  depends only on the initial state  $x(k|k)$  and on the actual and future control inputs :  $u(k|k), u(k+1|k), \dots, u(k+i-1|k)$ .

#### 4.3.1.2 Cost function and optimization problem

The MPC strategy is based on the optimization of a cost function defined over a finite time interval. A general formulation of this cost function can be expressed as:

$$J(U(k), x(k), k) = \Phi(x(k+N_p|k)) \sum_{i=0}^{N_p-1} \mathcal{L}(x(k+i|k), u(k+i|k)) \quad (4.7)$$

where:

- $N_p$  is the so called *Prediction Horizon*;
- $x(k+i|k)$  is the  $i^{\text{th}}$  step ahead state prediction obtained using model (4.5) and starting from the known initial state  $x(k|k) = x(k)$ ;
- $U(k) = [u(k|k), u(k+1|k), \dots, u(k+N_p-1|k)]^T$  is the vector of future control moves to be optimized;
- $\mathcal{L}(\cdot)$  is the per-stage cost function which defines the control objectives;
- $\Phi(\cdot)$  represents the final cost and takes into account that the prediction horizon is not infinite.

The functions  $\mathcal{L}(\cdot)$  and  $\Phi(\cdot)$  are assumed continuous in their arguments and are chosen according to the desired performance of the controlled system.

The general formulation of the optimal control problem to be solved is shown:

$$\begin{aligned}
 U^0(k|k) &= \arg \min_{U(k)} J(U(k), x(k)) \\
 \text{s.t. } \quad &x(k+1|k) = Ax(k) + Bu(k) \\
 &x(k+i|k) \in \mathcal{X}, \quad i = 1, \dots, N_p - 1 \\
 &u(k+i|k) \in \mathcal{U}, \quad i = 1, \dots, N_p - 1 \\
 &x(k+N_p|k) \in \mathcal{X}_{\mathcal{F}}
 \end{aligned} \tag{4.8}$$

where:

- $\mathcal{X}$  and  $\mathcal{U}$  are the input and state constraint sets respectively. While  $\mathcal{U}$  is chosen to introduce input actuator saturation and slew rate constraints,  $\mathcal{X}$  is chosen to impose limitations on state and/or output variables. The described sets are assumed to be convex and compact;
- $\mathcal{X}_{\mathcal{F}}$  is the terminal constraint set introduced in the optimization problem in order to ensure asymptotic stability [14];
- $U^0(k|k) = [u^0(k|k)^T, u^0(k+1|k)^T, \dots, u^0(k+N_p-1|k)^T]^T$  is the optimal input control sequence.

The choice of the cost function is of paramount importance in order to obtain a suitable MPC setup that allows the achievement of the control objectives. As an example, for the problem of zero regulation of the states, a typical choice is to express the weighting functions  $\mathcal{L}(\cdot)$  and  $\Phi(\cdot)$  in equation (4.7) as quadratic forms:

$$\begin{aligned}
 \mathcal{L}(\cdot) &= x(k+i|k)^T Q x(k+i|k) + u(k+i|k)^T R u(k+i|k), \quad i = 1, \dots, N_p - 1 \\
 \Phi(\cdot) &= x(k+N_p|k)^T P x(k+N_p|k)
 \end{aligned} \tag{4.9}$$

where  $Q \succeq 0$ ,  $R \succeq 0$  and  $P \succeq 0$  are suitable matrices.

Note that, the optimal input sequence  $U^0(k|k)$  has to be computed for all  $N_p$  future steps. For high values of  $N_p$ , the computational time needed to solve the optimal problem significantly increases and, in order to limit it, a possible solution is to optimize the cost function (4.7) with respect to the reduced sequence  $U'(k) = [u(k|k), u(k+1|k), \dots, u(k+N_c-1|k)]^T$ , where  $N_c < N_p$  is referred to as *Control Horizon*. In this case, the remaining  $N_p - N_c$  control input sequence  $U''(k) = [u(k+N_c|k), u(k+N_c+1|k), \dots, u(k+N_p-1|k)]^T$  needed to calculate the state predictions until the time step  $N_p$  is reached, can be chosen as:

- $u(k+i|k) = 0 \quad N_c \leq i \leq N_p - 1$ ;

- $u(k+i|k) = u(k+N_c|k) \quad N_c \leq i \leq N_p - 1$ ;
- $u(k+i|k) = -Fx(k+i|k) \quad N_c \leq i \leq N_p - 1$ , where  $F \in \mathbb{R}^{m \times n}$  represents a stabilizing state feedback gain.

Whenever the minimization problem (4.8) is characterized by a LTI prediction model (4.5), a quadratic cost function (4.9) and linear constraints expressed by the sets of inequalities  $\mathcal{X}$  and  $\mathcal{U}$ , the optimization is referred to as Quadratic Programming (QP) problem [15]. Indeed, it is proven that the cost function is quadratic with respect to the optimization variable  $U(k)$  on which also depend linear input/state constraints inequalities. In this regard, after some manipulation of the quadratic cost function and constraints, the original optimization problem (4.8) can be expressed as the following QP:

$$\begin{aligned} U^0(k|k) = \arg \min_{U(k)} J(U(k), x(k)) &= \arg \min_{U(k)} \frac{1}{2} U(k)^T H U(k) + x(k|k)^T F U(k) \\ \text{s.t. } LU(k) &\leq W \end{aligned} \quad (4.10)$$

In the considered setting, the QP problem is convex and the solution can be found through effective numerical algorithms [16].

#### 4.3.1.3 The Receding Horizon principle

From the solution of the problem (4.8) an optimal control sequence  $U^0(k|k)$  is obtained. The injection of this sequence to the system in evolution (4.5) defines an open-loop control strategy which is subject to the influence of uncertainties and disturbances leading the overall control system to poor performances. To overcome such a drawback, a feedback control action can be obtained through the so called Receding Horizon (RH) principle described by the following steps:

1. get the current state  $x(k|k)$ ;
2. solve the optimization problem (4.8) to get the minimizer  $U^0(k|k)$ ;
3. apply as present control action  $u(k) = u^0(k|k)$ , i.e. the only first component of the minimizer  $U^0(k|k)$ ;
4. repeat the entire procedure each time step.

Consequently, the RH principle implicitly defines a non-linear time invariant static state feedback control law (see Fig. 4.4) of the form:

$$U(k) = \mathcal{K}(x(k)) \quad (4.11)$$

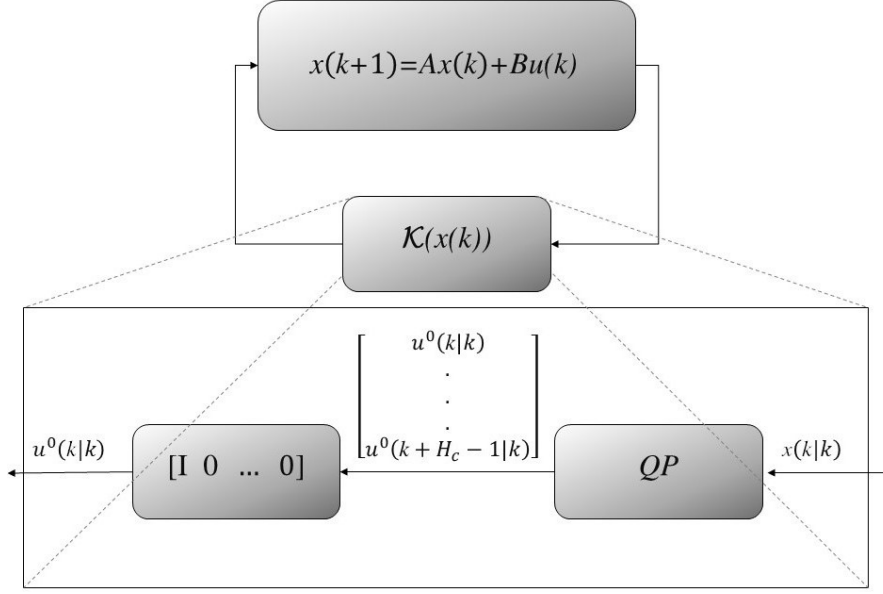


**Figure 4.4:** The RH controller  $\mathcal{K}(\cdot)$  as the solution of QP.

### 4.3.2 MPC for hybrid MLD systems

Optimal control for hybrid models can be formulated similarly to the one presented in section (4.3.1.2) for LTI systems. The literature is rich in approaches under the term of *Hybrid MPC*, nevertheless, for the present thesis purposes, the problem of Model Predictive Control formulation for MLD models will be addressed. In this context, recalling the MLD equations defined in (4.4), the predictions can be constructed exactly as in the linear case:

$$x(k+i|k) = A^i x(k|k) + \sum_{j=0}^{i-1} A^j (B_1 u_{i-1-j|k} + B_2 \delta_{i-1-j|k} + B_3 z_{i-1-j|k} + B_5) \quad (4.12)$$

where the state prediction  $x(k+1|k)$  depends on the initial state  $x(k|k)$  and on  $\xi(k) = [u(k|k), \dots, u(k+i-1|k), \delta(k|k), \dots, \delta(k+i-1|k), z(k|k), \dots, z(k+i-1|k)]$  sequence.

The problem of interest consists of finding the optimal triple referred as  $\xi^0(k|k) = [u^0(k)^T, \delta^0(k)^T, z^0(k)^T]^T$  minimizing the cost function shown below:

$$J(x(k), u(k), \delta(k), z(k)) = \|Px(N_p)\|_2 + \sum_{k=0}^{N_p-1} (\|Q(x(k))\|_2 + \|Ru(k)\|_2 + \|Q_\delta(\delta(k))\|_2 + \|Q_z(z(k))\|_2) \quad (4.13)$$

where  $P$  is the terminal cost and matrices  $Q$ ,  $R$ ,  $Q_\delta$  and  $Q_z$  weight each entry of the cost function  $J$  in 2-norm. The optimization problem is then expressed:

$$\begin{aligned}
 \xi^0(k|k) &= \arg \min_{\xi(k)} J(x(k), \xi(k)) \\
 \text{s.t. } \quad &x(k+1) = Ax(k) + B_1u(k) + B_2\delta(k) + B_3z(k) \\
 &y(k) = Cx(k) + D_1u(k) + D_2\delta(k) + D_3z(k) + D_5 \\
 &E_2\delta(k) + E_3z(k) \leq E_1u(k) + E_4x(k) + E_5 \\
 &x(k + N_p|k) \in \mathcal{X}_{\mathcal{F}} \\
 &x(k|k) = x(0)
 \end{aligned} \tag{4.14}$$

As the optimization vector  $\xi(k)$  encloses mixed real and binary components, the resulting optimization problem is referred to as Mixed-Integer Quadratic Programming (MIQP) which can be reformulated as follows:

$$\begin{aligned}
 \xi^0(k|k) &= \arg \min_{\xi(k)} J(x(k), \xi(k)) = \arg \min_{\xi(k)} \frac{1}{2} \xi(k)^T H \xi(k) + x(k|k)^T F \xi(k) \\
 \text{s.t. } \quad &G\xi(k) \leq W + Sx(k|k)
 \end{aligned} \tag{4.15}$$

where  $H$ ,  $F$ ,  $G$ ,  $W$  and  $S$  are matrices of suitable dimensions.

Binary constraints make MIP a hard problem to be handled, however, excellent general purpose branch & bound / branch & cut solvers are available for MIQP [17]. The *Gurobi*<sup>®</sup> solver [18] is employed in the optimization problem of the present thesis.

### 4.3.3 Actuator delay effects

In the following sections it will be described how the general formulation of MPC can be customized in order to improve the overall feedback control system performance.

As a first step, the actuator delay effect can be taken into account by modifying the state equation (4.5) as:

$$\begin{aligned}
 x(k+1) &= Ax(k) + Bu(k - \tau_d k) \\
 y(k) &= Cx(k)
 \end{aligned} \tag{4.16}$$

where  $\tau_d$  represents the number of time steps corresponding to the input delay. Since the presence of this latter may lead to the system instability, it is convenient to include the input delay effects in the prediction. This can be done by mapping the delay steps as poles in zero ( $z = 0$ ) and representing them as  $\tau_d$  new states  $x_{\tau_d}(k)$  so that:

$$x_h(k) = u(k - h), \quad h = 1, \dots, \tau. \tag{4.17}$$

Thus, considering the augmented state:

$$\tilde{x}(k) = [x(k), x_{\tau_d}(k), x_{\tau_d-1}(k), \dots, x_1(k)]^T, \quad (4.18)$$

the augmented LTI system used for prediction becomes:

$$\tilde{x}(k+1) = \begin{bmatrix} A & B & 0 & 0 & \dots & 0 \\ 0 & 0 & 1 & 0 & \dots & 0 \\ 0 & 0 & 0 & 1 & \dots & 0 \\ \vdots & \vdots & \vdots & \ddots & & \vdots \\ 0 & 0 & 0 & 0 & \dots & 0 \end{bmatrix} \begin{bmatrix} x(k) \\ x_{\tau_d}(k) \\ x_{\tau_d-1}(k) \\ \vdots \\ x_1(k) \end{bmatrix} + \begin{bmatrix} 0 \\ 0 \\ 0 \\ \vdots \\ 1 \end{bmatrix} u(k) \quad (4.19)$$

#### 4.3.4 Tracking problem

As a second step, the output tracking problem is considered. The cost function can be modified to make the measured outputs of the system to track a specific known reference referred to as  $y^0(k)$ .

$$\begin{aligned} J(U(k), x(k)) &= \sum_{i=0}^{N_p-1} (y^0(k+i|k) - y(k+i|k))^T Q (y^0(k+i|k) - y(k+i|k)) + \\ &\quad + u(k+i|k)^T R u(k+i|k) = \\ &= \sum_{i=0}^{N_p-1} (y^0(k+i|k) - Cx(k+i|k))^T Q (y^0(k+i|k) - Cx(k+i|k)) + \\ &\quad + u(k+i|k)^T R u(k+i|k) \end{aligned} \quad (4.20)$$

The minimization of this cost function allows the zero regulation of the tracking error  $e_t(k) = \|y^0(k) - y(k)\|$ . However, it is well known [14] that such minimization even for a constant reference tracking could result in a steady state error due to the presence of uncertainty on the system. A possible strategy to improve the tracking performance is described in the next section.

#### 4.3.5 Integral action

A standard approach to eliminate steady state errors in the presence of constant references and/or constant additive disturbances is to use the integral action. In the MPC tracking problem, the integral of the tracking errors  $q(k)$  is introduced as an extra state variable in discrete-time form:

$$q(k+1) = q(k) + e_t(k) \quad (4.21)$$

where the tracking error is given by  $e_t(k) = y^0(k) - y(k) = y^0(k) - Cx(k)$ . In order to consider the presence of the integral state in the prediction model, the augmented state  $\tilde{x} = [x(k), y^0(k), q(k)]^T$  is introduced. The state-space equations (4.5) becomes:

$$\begin{aligned} \tilde{x}(k+1) &= \begin{bmatrix} A & 0 & 0 \\ 0 & 0 & I \\ -C & I & I \end{bmatrix} \begin{bmatrix} x(k) \\ y^0(k) \\ q(k) \end{bmatrix} + \begin{bmatrix} B \\ 0 \\ 0 \end{bmatrix} u(k) \\ y(k) &= \begin{bmatrix} C & 0 & 0 \end{bmatrix} \begin{bmatrix} x(k) \\ y^0(k) \\ q(k) \end{bmatrix} \end{aligned} \quad (4.22)$$

The integral state  $q(k)$  can be taken into account in the cost function as:

$$\begin{aligned} J(U(k), x(k)) &= \sum_{i=0}^{N_p-1} (y^0(k+i|k) - y(k+i|k))^T Q_y (y^0(k+i|k) - y(k+i|k)) + \\ &\quad + q(k+i|k)^T Q_{int} q(k+i|k) + u(k+i|k)^T R u(k+i|k) \end{aligned} \quad (4.23)$$

where the effort of the integral action can be tuned through the entries of matrix  $Q_{int}$ . High  $Q_{int}$  values ensure that the tracking error quickly reaches zero with a strong control action. Nevertheless, the higher is the  $Q_{int}$ , the more aggressive is the system response.

## Chapter 5

# Micro-slip control system design

In order to study and develop a Hybrid MPC controller able to manage the clutch micro-slip problem, it is important to first analyze all the devices that are linked to the operation of the transmission system. Figure 5.1 shows a general scheme of the controlled transmission system useful to recognize all its components. Such components will be described individually in the following sections introducing their Simulink® blocks.

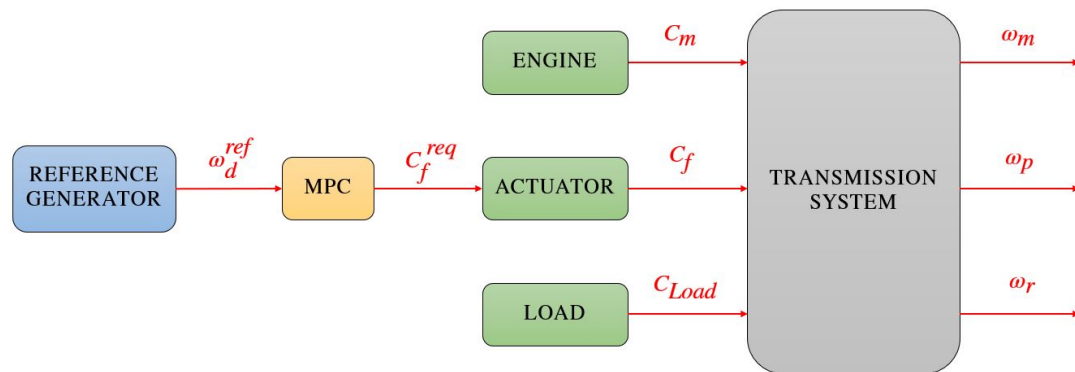


**Figure 5.1:** Micro-slip control architecture. The detailed non-linear transmission system outputs the only measurable velocities  $\omega_m$ ,  $\omega_p$  and  $\omega_r$ .

## 5.1 Engine

Under the assumption that the engine motion on its suspension is neglected, the engine block is modelled as a mean value torque generator which does not include high frequency transients. In general, the engine output torque  $C_m$  is considered as a function of the engine speed  $\omega_m$  and throttle position  $p$  in percentage of opening:

$$C_m = f(\omega_m, p), \quad (5.1)$$

nevertheless, for the sake of simplicity,  $C_m$  is assumed as a fixed signal, measurable in every sampling instant. Since simulations focus on the study of the odd-gear clutch K1, multiple engine torque profiles are proposed in Figure 5.2. More specifically, the considered torque profiles are based on experimental simulations in order to test the transmission system under different operating conditions.

## 5.2 Load effects

The vehicle load effects include the aerodynamic resistance force  $F_a$ , the rolling resistance force  $F_r$  and the uphill driving force  $F_g$ . The aerodynamic resistance force is approximated by the relation:

$$F_a = \frac{1}{2} \rho_a A_f C_a (v_a + v_v)^2, \quad (5.2)$$

where  $\rho_a$  is the air density,  $A_f$  is the frontal area of the vehicle,  $C_a$  is the aerodynamic drag coefficient,  $v_a$  and  $v_v$  are the speeds of the wind and the vehicle, respectively. The rolling resistance force is modelled as:

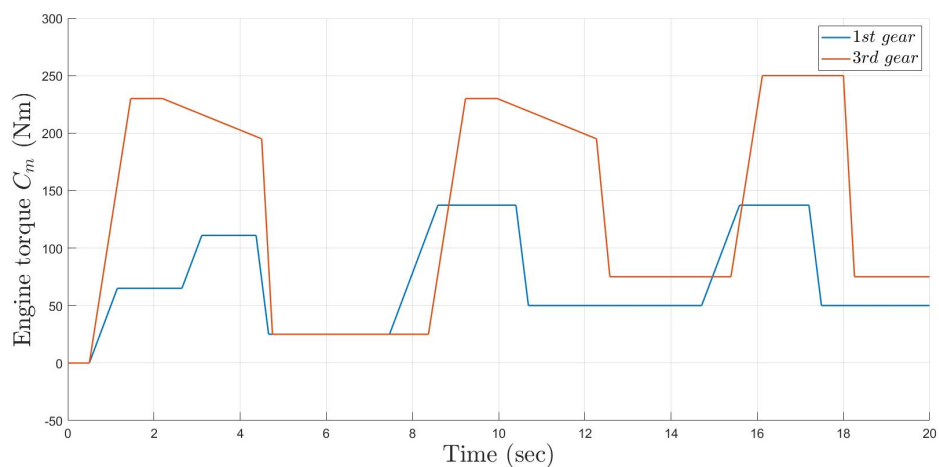
$$F_r = m_v g \mu_r \cos \beta, \quad (5.3)$$

where  $m_v$  is the vehicle mass,  $g$  is the gravitational acceleration,  $\mu_r$  is the rolling friction coefficient, and  $\beta$  is the slope angle of the road. The uphill driving force induced by gravity when driving on a non-horizontal road is:

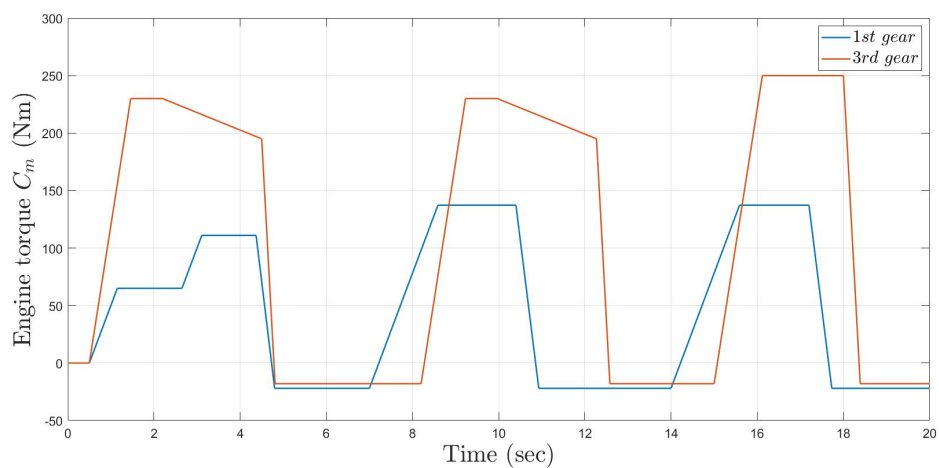
$$F_g = m_v g \mu_r \sin \beta, k \quad (5.4)$$

hence, considering the wheels radius  $r_W$ , the overall vehicle resistance torque  $C_{Load}$  can be expressed as:

$$C_{Load} = (F_a + F_r + F_g) r_W. \quad (5.5)$$



(a)



(b)

**Figure 5.2:** Engine torque profiles for first and third gear. Panel (a):  $C_m$  torques with partial release of the acceleration pedal. Panel (b):  $C_m$  torques with complete release of the acceleration pedal.

### 5.3 Actuator block

With regard to what has been said in section (3.2), the actuator block includes four main components:

- the subsystem  $G_{act}(s)$ , which contains the actuator transfer function experimentally obtained:

$$G_{act}(s) = \frac{C_f(s)}{C_f^{req}(s)} = \frac{18.572(s + 138)}{s^2 + 82.23s + 2563}; \quad (5.6)$$

- the *Actuator\_Delay* block that takes into account the delayed action of the actuator assumed to be equal to 10ms;
- the *Saturation* block that fixes the upper and lower bounds of the transmitted torque  $C_f$ ;
- the *Transmissibility* block, which accounts for the  $K_t$  transmissibility coefficient variations.

The overall actuator block scheme is depicted in Figure (5.3)

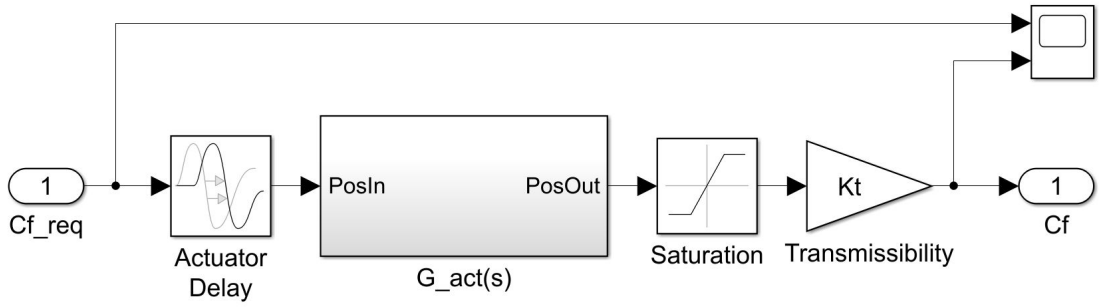


**Figure 5.3:** Actuator block with  $Cf\_req$  as input and  $Cf$  as output.

## 5.4 Reference Generator

The Reference Generator (RG) block shown in Figure 5.4 outputs the reference signal  $\omega_d^{ref}$  that has to be tracked by the slipping speed  $\omega_d$ . Due to the considerations mentioned in section (3.4.1), such reference must be consistent with the current Mode of the PWA model (4.3), therefore, the RG operation can be resumed as follows:

$$\omega_d^{ref} = \begin{cases} ORef\_pos & C_m \geq 0 \\ ORef\_neg & C_m < 0, \end{cases} \quad (5.7)$$

where  $ORef_{pos}$  and  $ORef_{neg}$  are positive and negative constant references, respectively. Note that, the switching logic of the RG is managed by the sign inversion of the engine torque  $C_m$  (instead of  $\omega_d$ ), its knowledge is in fact assumed in advance in order to generate the proper reference signal before the controlled system changes its operating condition. In this context, the  $C_m$  Boolean signal that triggers the RG is introduced:

$$C_{m-mode} = \begin{cases} false & \text{if } C_m \geq 0 \\ true & \text{if } C_m < 0. \end{cases} \quad (5.8)$$

Another feature of the RG is the capability of generating an initial ramp signal useful to smooth  $\omega_d$  transients. Tuning parameters of the RG are summarized below:

- $ORef_{pos}$  and  $ORef_{neg}$  set the main reference values to be tracked as described previously;
- $ORef_{slope\_pos}$  and  $ORef_{slope\_neg}$  fix the slope of the connecting ramp between the two constant reference values mentioned above;
- $ORef_{slope0}$  defines the slope of the initial ramp;
- $ORef_0$  adjusts the starting point of the initial ramp.

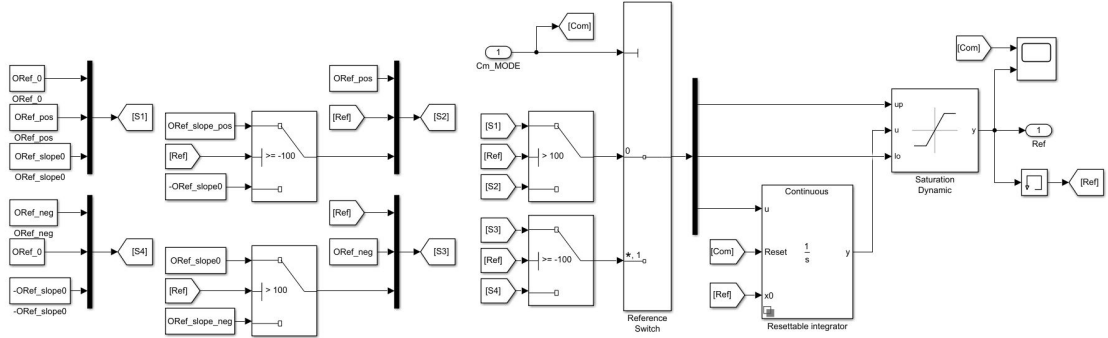


**Figure 5.4:** Reference Generator (RG) block.

As mentioned previously, a slight slipping of the clutch plates must be assured in order to guarantee comfort and to avoid increases of the clutch wear. The choice of the speed reference to track is of paramount importance in this context. Then,

for the considered problem, the following RG settings have been chosen:

$$\begin{aligned}
 ORef\_pos &= 100 \text{ rpm} \\
 ORef\_neg &= -100 \text{ rpm} \\
 ORef\_slope\_pos &= 50 \text{ rpm/ms} \\
 ORef\_slope\_neg &= -50 \text{ rpm/ms} \\
 ORef\_slope0 &= 0.98 \text{ rpm/ms}
 \end{aligned} \tag{5.9}$$

## 5.5 Hybrid MPC design

The design of the present hybrid micro-slip MPC controller takes into account two main conflicting objectives:

- the accurate reference tracking of the clutch slipping speed  $\omega_d = \omega_m - \omega_p$ ;
- the attenuation of torsional oscillations inside the driveline through the zero regulation of the torsion speed  $\omega_{sr} = \frac{\omega_p}{\tau} - \omega_r$ .

Moreover, unlike standard MPC approaches, the introduction of the hybrid framework allows the controller to handle the non-linear dynamic of the system presented in section (3.4.1), guaranteeing the satisfaction of the objectives stated above. Further features of the adopted MPC include constraints on the minimum and maximum actuated clutch torque  $C_f$ .

### 5.5.1 Transmission predictive model

The Hybrid MPC predictive model is composed by the union of the actuator and driveline models, as shown in Figure (5.5).

The actuator system model can be formulated as:

$$\begin{aligned}
 x_{act}(k+1) &= A_{act}x_{act}(k) + B_{act}u(k) \\
 y_{act}(k) &= C_{act}x_{act}(k)
 \end{aligned} \tag{5.10}$$

where:

- $x_{act}(k) = [x_{act1}(k), x_{act2}(k)]^T$  is the actuator state vector;
- $u(k)$  is the control input  $C_f^{req}(k)$  computed by the MPC controller;
- $y_{act}(k)$  is the effective clutch torque  $C_f(k)$  applied to the driveline;
- the matrices  $A_{act}$ ,  $B_{act}$  and  $C_{act}$  are expressed in the canonical control form starting from the actuator transfer function (5.6).

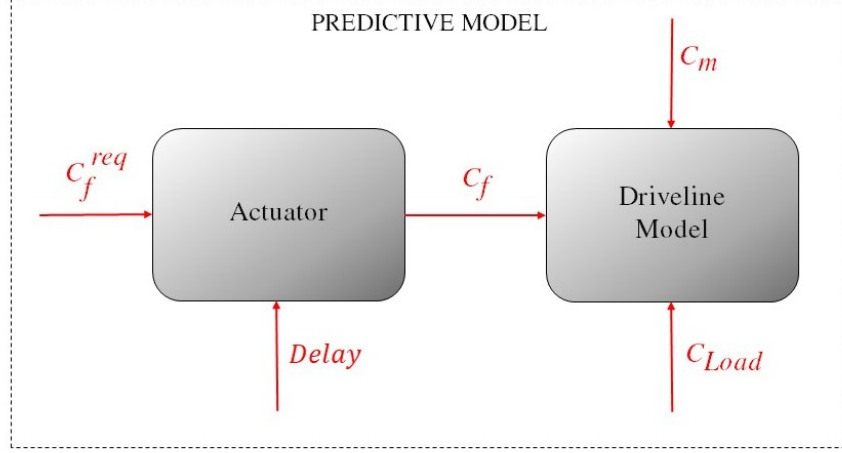


**Figure 5.5:** Predictive model scheme.

Besides, the actuator has a delay of 10 ms that corresponds exactly to one sampling time of the system. Hence, as explained in section (4.3.3), in order to consider its effects in the prediction, the state equations (5.10) are augmented as follows:

$$\begin{aligned}\tilde{x}_{act}(k+1) &= \tilde{A}_{act}\tilde{x}_{act}(k) + \tilde{B}_{act}u(k) \\ \tilde{y}_{act}(k) &= \tilde{C}_{act}\tilde{x}_{act}(k)\end{aligned}\tag{5.11}$$

where:

- $\tilde{x}_{act}(k) = [x_{act1}(k), x_{act2}(k), x_\tau(k)]^T$  is the augmented state vector;
- $x_\tau(k) = u(k - T_s) = C_f^{req}(k - T_s)$  is the one-sample delayed input;
- $\tilde{A}_{act} = \left[ \begin{array}{c|c} A_{act} & B_{act} \\ \hline 0 & 0 \end{array} \right]$ ,  $\tilde{B}_{act} = \left[ \begin{array}{c} 0 \\ 1 \end{array} \right]$ ,  $\tilde{C}_{act} = [C_{act} \ 0]$ .
- the matrices  $A_{act}$ ,  $B_{act}$  and  $C_{act}$  are expressed in the canonical control form starting from the actuator transfer function (5.6).

The driveline discrete state-space representation is recalled from section (4.1.2.1), where matrices  $A_{cd}$ ,  $B_{cd}$ ,  $C_{cd}$  are obtained through a zero-order hold discretization of the system (3.3) input with a sampling time of  $T_s = 10$  ms.

The points below discuss the further steps performed to derive a suitable prediction model to be employed in the MPC design.

1. The driveline PWA model (4.3) is combined with the augmented actuator system (5.11) so that the overall system is expressed in PWA form. The following assumptions hold:

- the output of the actuator is the input of the driveline system;
- the engine torque  $C_m(k)$  and the load torque  $C_{Load}(k)$  are measurable at the current time  $k$ . Thus, in order to take into account their effects, they are considered as two additional states whose evaluations within the prediction horizon are kept constant and equal to the measured one at time  $k$ .

The overall system is reformulated as follows:

$$\begin{cases} \check{x}(k+1) = \check{A}(\alpha(k))\check{x}(k) + \check{B}u(k) \\ \check{y}(k) = \check{C}\check{x}(k) \\ \alpha(k) = \begin{cases} 1 & \text{if } \omega_d(k) \geq 0, & \text{Mode 1} \\ -1 & \text{if } \omega_d(k) < 0, & \text{Mode 2} \end{cases} \end{cases} \quad (5.12)$$

with:

$$\check{x}(k) = \begin{bmatrix} x_{act1}(k) & x_{act2}(k) & x_\tau(k) & \omega_m(k) & \omega_p(k) & \omega_r(k) \\ \omega_{sr}(k) & C_m(k) & C_{Load}(k) \end{bmatrix}^T \quad (5.13)$$

and:

$$\check{A} = \left[ \begin{array}{c|c|c|c} \check{A}_{act} & 0 & 0 & 0 \\ \hline \alpha(k)B_{cd}(i,2)\check{C}_{act} & A_{cd} & B_{cd}(i,1) & B_{cd}(i,3) \\ \hline 0 & 0 & 1 & 0 \\ \hline 0 & 0 & 0 & 1 \end{array} \right]_{i=1, \dots, 4} \quad (5.14)$$

$$\check{B} = [0 \ 0 \ 1 \ 0 \ 0 \ 0 \ 0 \ 0 \ 0]^T$$

$$\check{C} = \begin{bmatrix} 0 & 0 & 0 & 1 & -1 & 0 & 0 & 0 & 0 \\ 0 & 0 & 0 & 0 & \frac{1}{\tau} & -1 & 0 & 0 & 0 \end{bmatrix}$$

2. The slipping speed reference  $\omega_d^{ref}(k)$ , the tracking error  $e_t(k)$  and the integral action  $q(k)$  are added as additional states to the system (5.12) using the techniques introduced in sections (4.3.4) and (4.3.5). More precisely,  $\omega_d^{ref}(k)$

evolution is assumed to be constant during the entire prediction horizon  $N_p$ , obtaining:

$$\begin{cases} x_{pred}(k+1) = A_{pred}(\alpha(k))x_{pred}(k) + B_{pred}u(k) \\ y_{pred}(k) = C_{pred}x_{pred}(k) \\ \alpha(k) = \begin{cases} 1 & \text{if } \omega_d(k) \geq 0, & \text{Mode 1} \\ -1 & \text{if } \omega_d(k) < 0, & \text{Mode 2} \end{cases} \end{cases} \quad (5.15)$$

with:

$$x_{pred}(k) = \begin{bmatrix} x_{act1}(k) & x_{act2}(k) & x_\tau(k) & \omega_m(k) & \omega_p(k) & \omega_r(k) \\ \omega_{sr}(k) & \omega_d^{ref}(k) & e_t(k) & q(k) & C_m(k) & C_{Load}(k) \end{bmatrix}^T \quad (5.16)$$

and:

$$A_{pred} = \left[ \begin{array}{c|ccc|cc} \tilde{A}_{act} & 0 & 0 & 0 & 0 & 0 & 0 \\ \hline \alpha(k)B_{cd}(i,2)\tilde{C}_{act} & A_{cd} & 0 & 0 & 0 & B_{cd}(i,1) & B_{cd}(i,3) \\ \hline 0 & 0 & 1 & 0 & 0 & 0 & 0 \\ v_1 & v_2 & 1 & 0 & 0 & v_3 & v_4 \\ v_1 & v_2 & 1 & 0 & 1 & v_3 & v_4 \\ \hline 0 & 0 & 0 & 0 & 0 & 1 & 0 \\ 0 & 0 & 0 & 0 & 0 & 0 & 1 \end{array} \right] \quad i = 1, \dots, 4$$

$$B_{pred} = \begin{bmatrix} 0 & 0 & 1 & 0 & 0 & 0 & 0 & 0 & 0 & 0 & 0 & 0 \end{bmatrix}^T$$

$$C_{pred} = \begin{bmatrix} 0 & 0 & 0 & 1 & -1 & 0 & 0 & 0 & 0 & 0 & 0 & 0 \\ 0 & 0 & 0 & 0 & \frac{1}{\tau} & -1 & 0 & 0 & 0 & 0 & 0 & 0 \end{bmatrix} \quad (5.17)$$

where:

$$\begin{aligned} v_1 &= -C_{cd}(1, j)\alpha(k)B_{cd}(i, 2)C_{act} \\ v_2 &= -C_{cd}(1, j)A_{cd} & i = 1, \dots, 4 \\ v_3 &= -C_{cd}(1, j)B_{cd}(i, 1) & j = 1, \dots, 4 \\ v_4 &= -C_{cd}(1, j)B_{cd}(i, 3) \end{aligned}$$

Finally, the behavior of the switching variable  $\alpha(k)$  is translated in terms of a logic signal  $\omega_{d-mode}$  as described below:

$$\omega_{d-mode} = \begin{cases} false & \text{if } \omega_d \geq 0 \\ true & \text{if } \omega_d < 0. \end{cases} \quad (5.18)$$

## 5.5.2 Cut-off logic

The PWA model (5.15) is implemented through the HYSDEL descriptor in order to derive a MLD object suitable for optimization problems. Nevertheless, further manipulations of the predictive model are required in order to cope with technical issues occurring during the slipping speed zero-crossing phase. Indeed, it has been observed that the presence of a residual clutch torque during switching may cause chattering phenomena for the computed input torque leading to bang-bang behaviors of the slipping speed trajectory. Such phenomena are motivated by the introduction of a strong non-linearity inside the driveline dynamics. A possible solution to this problem includes the definition of a *cut-off* region inside which the control input  $C_f^{req}$  is set to zero. Consequently, a Boolean signal  $cut-off_{mode}$  is formulated such that it is triggered during particular operative conditions:

- every time the engine torque  $C_m$  and the slipping speed  $\omega_d$  have opposite signs;
- whenever the slipping speed is confined inside a user-defined region.

Recalling the binary signals (5.8) and (5.18), the  $cut-off_{mode}$  operation is described by the following relations:

$$cut-off_{mode} = \neg\omega_{d-mode} \wedge C_{m-mode} \vee \omega_{d-mode} \wedge \neg C_{m-mode} \vee T_{hl-mode} , \quad (5.19)$$

where the logic signal  $T_{hl-mode}$  behaves as follows:

$$T_{hl-mode} = \begin{cases} true & \text{if } T_l \leq \omega_d \leq T_h \\ false & \text{elsewhere.} \end{cases} \quad (5.20)$$

The  $T_h$  and  $T_l$  thresholds are configurable constants introduced to further improve the robustness of the cut-off region. The functioning of both the  $cut-off_{mode}$  and  $\omega_{d-mode}$  logics is described by the Event Generator outlined in section (4.1.1) which can be implemented inside the *DA* section of the HYSDEL predictive model description. However, in order speed up simulations, an external EG is assumed so that two extra Boolean inputs need to be included as fictitious states inside the predictive model (5.15) with the following simple dynamics:

$$\begin{aligned} \omega_{d-mode}(k+1) &= \omega_{d-mode}(k) \\ cut-off_{mode}(k+1) &= cut-off_{mode}(k). \end{aligned} \quad (5.21)$$

The formulation of the system (5.15) together with the inclusion of the dynamics of the logic states (5.21) is the one actually used as predictive model in the simulations presented in Chapter 6.

### 5.5.3 Transmission cost function and optimization

The choice of a proper cost function is of paramount importance in order to satisfy the objectives stated in section (5.5). In particular, a quadratic cost function is adopted in the form:

$$J(x(k), U(k), \delta(k), z(k)) = \sum_{i=0}^{N_p-1} q_{\omega_d} e_t(k+i|k)^2 + q_{\omega_{sr}} \omega_{sr}(k+i|k)^2 + q_{int} q(k+i|k)^2 + RC_f^{req}(k+i|k)^2, \quad (5.22)$$

where:

- $q_{\omega_d}$  weights the tracking error  $e_t(k) = \omega_d^{ref}(k) - \omega_d(k)$ ;
- $q_{\omega_{sr}}$  weights the zero regulation of the torsion speed  $\omega_{sr}(k)$ ;
- $q_{int}$  is the weight of the integral state  $q(k)$ ;
- the weight  $R$  is just a scalar since the only manipulable control input is the requested clutch torque  $C_f^{req}$ .

The cost function (5.22) can be recast in the standard quadratic form (4.13):

$$J(x(k), U(k), \delta(k), z(k)) = \sum_{i=0}^{N_p-1} x(k+i|k)^T Q x(k+i|k) + u(k+i|k)^T R u(k+i|k), \quad (5.23)$$

where the state prediction vector  $x(k+i|k)$  is expressed by the equation (4.12) and includes both the continuous (5.16) and binary states (5.21). Besides, no weights on the auxiliary continuous and binary variables are considered – i.e.  $Q_z = Q_\delta = 0$ . Note that, in order to regulate  $\omega_{sr}$  to zero, the weight  $q_{\omega_{sr}}$  should be inserted inside precise positions of the matrix  $Q$ . Therefore, it is necessary to rearrange the following quadratic term:

$$q_{\omega_{sr}} \omega_{sr}^2 = q_{\omega_{sr}} \left( \frac{\omega_p}{\tau} - \omega_r \right)^2 = q_{\omega_{sr}} \left( \frac{\omega_p^2}{\tau^2} - \frac{2}{\tau} \omega_p \omega_r + \omega_r^2 \right), \quad (5.24)$$

in matrix form:

$$\begin{bmatrix} \omega_p & \omega_r \end{bmatrix} \begin{bmatrix} a & b \\ c & d \end{bmatrix} \begin{bmatrix} \omega_p \\ \omega_r \end{bmatrix} = a\omega_p^2 + c\omega_p\omega_r + b\omega_p\omega_r + d\omega_r^2. \quad (5.25)$$

By comparing equations (5.24) and (5.25) the values of the coefficients  $a$ ,  $b$ ,  $c$  and  $d$  are given by:

$$\begin{aligned} a &= \frac{q_{\omega_{sr}}}{\tau^2} \\ b &= c = -\frac{q_{\omega_{sr}}}{\tau} \\ d &= q_{\omega_{sr}}. \end{aligned} \quad (5.26)$$

The  $Q$  matrix final form is then presented:

$$Q = \begin{bmatrix} 0 & 0 & 0 & 0 & 0 & 0 & 0 & 0 & 0 & 0 & 0 & 0 & 0 & 0 \\ 0 & 0 & 0 & 0 & 0 & 0 & 0 & 0 & 0 & 0 & 0 & 0 & 0 & 0 \\ 0 & 0 & 0 & 0 & 0 & 0 & 0 & 0 & 0 & 0 & 0 & 0 & 0 & 0 \\ 0 & 0 & 0 & 0 & 0 & 0 & 0 & 0 & 0 & 0 & 0 & 0 & 0 & 0 \\ 0 & 0 & 0 & 0 & \frac{q_{\omega_{sr}}}{\tau^2} & -\frac{q_{\omega_{sr}}}{\tau} & 0 & 0 & 0 & 0 & 0 & 0 & 0 & 0 \\ 0 & 0 & 0 & 0 & -\frac{q_{\omega_{sr}}}{\tau} & q_{\omega_{sr}} & 0 & 0 & 0 & 0 & 0 & 0 & 0 & 0 \\ 0 & 0 & 0 & 0 & 0 & 0 & 0 & 0 & 0 & 0 & 0 & 0 & 0 & 0 \\ 0 & 0 & 0 & 0 & 0 & 0 & 0 & 0 & 0 & 0 & 0 & 0 & 0 & 0 \\ 0 & 0 & 0 & 0 & 0 & 0 & 0 & 0 & q_{\omega_d} & 0 & 0 & 0 & 0 & 0 \\ 0 & 0 & 0 & 0 & 0 & 0 & 0 & 0 & 0 & q_{int} & 0 & 0 & 0 & 0 \\ 0 & 0 & 0 & 0 & 0 & 0 & 0 & 0 & 0 & 0 & 0 & 0 & 0 & 0 \\ 0 & 0 & 0 & 0 & 0 & 0 & 0 & 0 & 0 & 0 & 0 & 0 & 0 & 0 \\ 0 & 0 & 0 & 0 & 0 & 0 & 0 & 0 & 0 & 0 & 0 & 0 & 0 & 0 \\ 0 & 0 & 0 & 0 & 0 & 0 & 0 & 0 & 0 & 0 & 0 & 0 & 0 & 0 \end{bmatrix} \quad (5.27)$$

where the weights  $R$ ,  $q_{\omega_d}$ ,  $q_{\omega_{sr}}$  and  $q_{int}$  are project parameters which can be modified to tune the MPC controller.

As previously discussed, the advantage of using a MPC controller lies in the possibility of including constraints for input and states during the computation of an optimal solution. In this regard, in order to take into account the physical limitation of the actuator, a constraint on the control input and the actuated clutch torque  $C_f$  are added:

$$\begin{aligned} C_f^{req} &\geq 0, \quad i = 1, \dots, N_{p-1}, \\ 0 &\leq C_f \leq 350Nm, \quad i = 1, \dots, N_{p-1}. \end{aligned} \quad (5.28)$$

More precisely, the inequality (5.28) is a state constraint and since no information about the real applied torque is given, an estimation of such quantity is needed (the problem of states estimation is addressed in the next section).

Finally, the expression of the overall optimization problem for the considered

transmission system is given by:

$$\begin{aligned}
 U^0(k|k) &= \arg \min_{U(k)} J(x(k), U(k)) \\
 \text{s.t.} \quad & \text{MLD equations of (5.15) and (5.21)} \\
 & C_f \leq 350, \quad i = 1, \dots, N_{p-1} \\
 & -C_f \leq 0, \quad i = 1, \dots, N_{p-1} \\
 & -C_f^{req} \leq 0, \quad i = 1, \dots, N_{p-1} \\
 & x(k|k) = x(0).
 \end{aligned} \tag{5.29}$$

Since the minimization problem involves mixed-integer linear relations, the optimization problem (5.29) is a MIQP.

### 5.5.4 Hybrid Kalman filter

Until now, it has been supposed that all the state variables are measurable. However, in most applications the quantities that are available for measurements are a subset of the variables required to model the system. Therefore, a State Observer (SO) is needed in order to provide an estimate  $\hat{x}(k)$  of the system states  $x(k)$  [19]. A general observer structure is reported Figure 5.6.

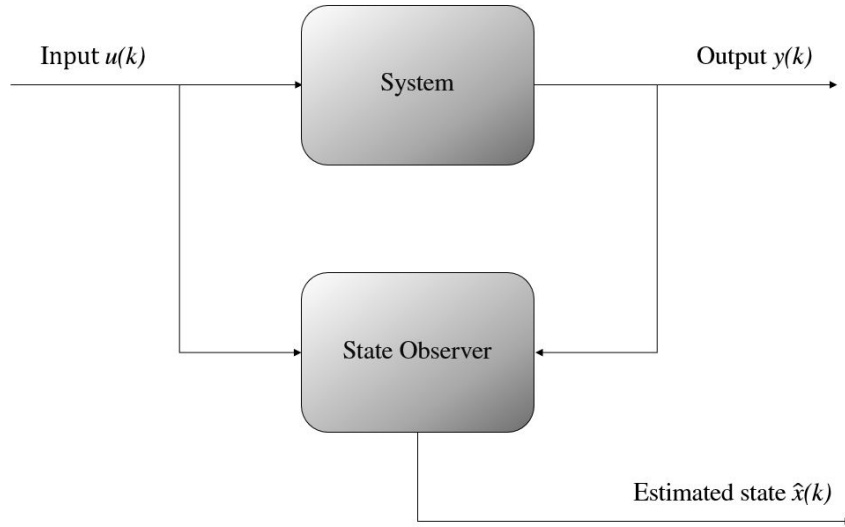


**Figure 5.6:** State Observer scheme.

The driveline state-space model (4.2) is characterized by four states of which three are measurable ( $\omega_m(k)$ ,  $\omega_p(k)$  and  $\omega_r(k)$ ) and one has to be estimated ( $\omega_{sr}(k)$ ).

Besides, as far as the actuator model (5.10) is concerned, the evaluation of the two actuator states  $x_{act1}(k)$  and  $x_{act2}(k)$  is needed in order to reconstruct an estimation of the actuated clutch torque  $C_f$ . Note that, since an hybrid description of the driveline equations is considered, the resultant SO will be formulated in PWA form. Consequently, knowing the inputs  $C_m$ ,  $C_f^{req}$  and  $C_{Load}$  the state equations of the augmented PWA system to be used for the development of the hybrid SO are derived:

$$\begin{cases} x_{est}(k+1) = A_{est}(\alpha(k))x_{est}(k) + B_{est}u(k) \\ y_{est}(k) = C_{est}x_{est}(k) \\ \alpha(k) = \begin{cases} 1 & \text{if } \omega_d(k) \geq 0, & \text{Mode 1} \\ -1 & \text{if } \omega_d(k) < 0, & \text{Mode 2} \end{cases} \end{cases} \quad (5.30)$$

with:

$$x_{est}(k) = [x_{act1}(k) \ x_{act2}(k) \ \omega_m(k) \ \omega_p(k) \ \omega_r(k) \ \omega_{sr}(k)]^T \quad (5.31)$$

and:

$$\begin{aligned} A_{est} &= \left[ \begin{array}{c|c} A_{act} & 0 \\ \alpha(k)B_{cd}(i,2)C_{act} & A_{cd} \end{array} \right] i = 1, \dots, 4 \\ B_{est} &= \left[ \begin{array}{c|c|c} 0 & B_{act} & 0 \\ B_{cd}(i,1) & 0 & B_{cd}(i,3) \end{array} \right] i = 1, \dots, 4 \\ C_{est} &= \begin{bmatrix} 0 & 0 & 1 & 0 & 0 & 0 \\ 0 & 0 & 0 & 1 & 0 & 0 \\ 0 & 0 & 0 & 0 & 1 & 0 \end{bmatrix} \end{aligned} \quad (5.32)$$

The augmented PWA system defined above is then used to formulate the asymptotic SO equations:

$$\begin{cases} \hat{x}_{SO}(k+1) = (A_{est}(\alpha(k)) - L(\alpha(k))C_{est})\hat{x}_{SO}(k) + B_{est}u(k) + L(\alpha(k))y_{est}(k) \\ \hat{y}_{SO}(k) = I_6\hat{x}_{SO}(k) \\ \alpha(k) = \begin{cases} 1 & \text{if } \omega_d(k) \geq 0, & \text{Mode 1} \\ -1 & \text{if } \omega_d(k) < 0, & \text{Mode 2} \end{cases} \end{cases} \quad (5.33)$$

If the couple  $(A_{est}, C_{est})$  is observable or at least detectable then a suitable gain  $L$  can be found so that the matrix  $[A_{est} - LC_{est}]$  is asymptotically stable. It is worth noting that sometimes a different approach can be used: it is possible to design a “reduced” order SO that estimates the unmeasured states only. Nevertheless, a full SO is considered (all the six states are output) in order to take advantage

of the filtering action that the observer performs on the noise of the measured states. The  $L$  matrix, which depends on the current Mode of the system (5.33), is derived using the Kalman filter approach. Hence two weight matrices  $\tilde{Q}$  and  $\tilde{R}$  with suitable dimensions are defined to tune the Kalman SO:

$$\begin{aligned} \tilde{Q} &= \begin{bmatrix} q_{SO} & 0 \\ 0 & q_{SO} \end{bmatrix} \\ \tilde{R} &= \begin{bmatrix} r_{SO} & 0 & 0 \\ 0 & r_{SO} & 0 \\ 0 & 0 & r_{SO} \end{bmatrix} \end{aligned} \tag{5.34}$$

where  $q_{SO}$  and  $r_{SO}$  entries establish whether to trust on the model or measurements. The SO PWA system (5.33) is modelled through HYSDEL with the inclusion of an extra Boolean input that is the logic signal (5.18). Such strategy is adopted in order to communicate to the hybrid observer on which operating condition it is working on.

# Chapter 6

## Simulation results

In this chapter extensive simulations on the proposed micro-slip control approach are conducted. More precisely, suitable tests have been performed on both first and third gears which belong to the odd-gear clutch K1. Simulations are carried out both in nominal and perturbed conditions in which a hybrid Kalman filter is employed.

All the simulations make usage of the Hybrid toolbox [20] for hybrid systems modeling and the Multi-Parametric Toolbox (MPT) [21] for the implementation of the hybrid MPC controller.

### 6.1 Tests without state observer

This section shows simulations performed using the nominal values of the physical parameters and in the absence of the measurement noises with a true state feedback. Before carrying out tests in different operating conditions a tuning procedure of the hybrid MPC controller is required. The tuning process concerns the choice of the prediction horizon  $N_p$ , the control horizon  $N_c$  and the weights  $q_{\omega_d}$ ,  $q_{\omega_{sr}}$ ,  $q_{int}$  and  $R$  of the quadratic cost function introduced in section (5.5.3):

$$J(x(k), U(k), \delta(k), z(k)) = \sum_{i=0}^{N_p-1} q_{\omega_d} e_t(k+i|k)^2 + q_{\omega_{sr}} \omega_{sr}(k+i|k)^2 + q_{int} q(k+i|k)^2 + RC_f^{req}(k+i|k)^2$$

At the beginning of the tuning procedure,  $N_p$  is chosen to be sufficiently long with respect to the dominant system dynamics, while  $N_c$  is assumed to be equal to  $N_p$ . The scalar weight  $R$  and the entries of the weight matrix  $Q$  are initially chosen in order to equally weight each term of the cost function. Then, each coefficient has been modified until a satisfactory trade-off among the obtained performances is

achieved. It is important to note that, since the engaged gear is known, a different MPC tuning can be applied to each gear. Consequently, the values of the design parameters have been collected in Table 6.1.

**Table 6.1:** Hybrid MPC design parameters.

Design parameters	1st gear	3rd gear
$N_p$	20	20
$q_{\omega_d}$	5	380
$q_{\omega_{sr}}$	1	120
$q_{int}$	1	0.1
$R$	60	20

The following simulations compare tip-in and tip-out maneuvers with partial and full releases of the acceleration pedal in order to show the correct operation of the hybrid MPC controller whenever the sign inversion of the slipping speed  $\omega_d$  occurs. In this regard, the settings of the RG (5.9) and the engine torque profiles shown in section (5.1) are considered. The tests are divided in two points: the former analyzes the dominant quantities of the transmission system with first gear engaged, the second point shows the same results for the third gear.

1. Figures 6.1 and 6.2 show the slipping speed reference tracking with engine torque  $C_m$  profiles resulting from partial (5.2)(a) and full (5.2)(b) release of the throttle pedal respectively, while Figures 6.3 and 6.4 display the corresponding torsion oscillations  $\omega_{sr}$ .

As it can be seen from the above simulations, the performance obtained with the first gear engaged is quite poor in terms of tracking, however, as shown in Figure (6.2), the hybrid MPC controller is able to effectively manage the two operating regions (Mode 1 and Mode 2) of the slipping speed.

As far as torsion oscillations concern, despite some "peaks" in correspondence of the high slopes of the engine torque, the trend of  $\omega_{sr}$  lies within an acceptable range of values with relatively few fluctuations.

It is also important to describe the behavior of the longitudinal acceleration  $a_x$  shown in Figures 6.5 and 6.6. Such quantity allows to go back to an estimate of the trend of the oscillations inside the transmission shaft. In fact, a common problem encountered during the design procedure is related to the information about  $\omega_{sr}$  which is often not available, nevertheless, through suitable mathematical transformations it can be linked to the longitudinal acceleration whose value can be easily obtained.

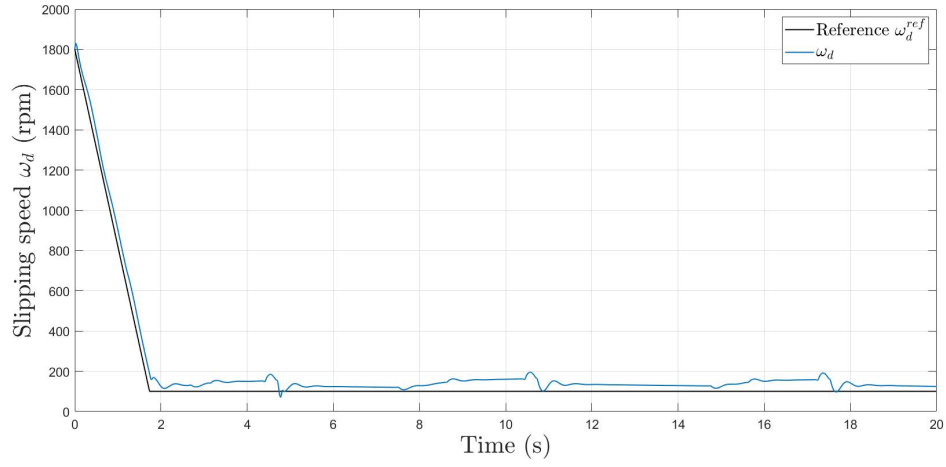


**Figure 6.1:** Slipping speed  $\omega_d$  with 1st gear engaged and partial release of the accelerator.

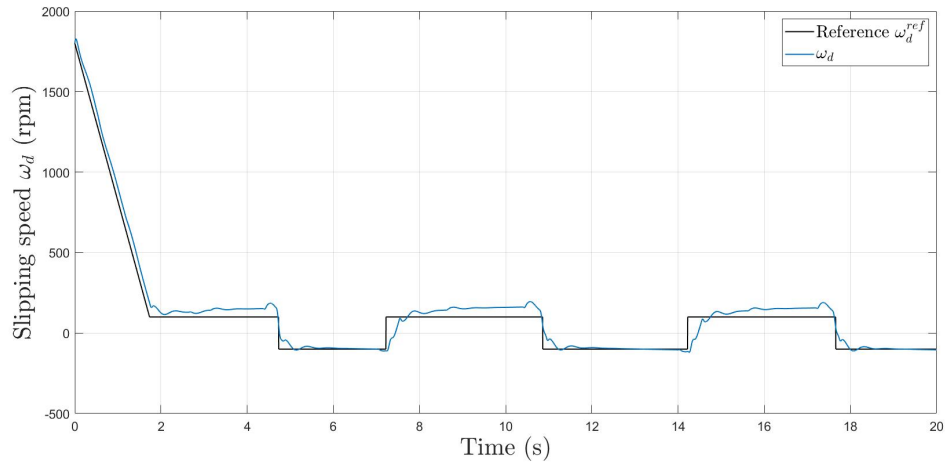


**Figure 6.2:** Slipping speed  $\omega_d$  with 1st gear engaged and full release of the accelerator.

2. The same tests conducted previously for the first gear are reproduced below for the third gear with the corresponding engine torque profiles (5.2)(a) and (5.2)(b). Figures 6.7 and 6.8 show an accurate tracking of the slipping speed reference as for the  $\omega_{sr}$  zero-regulation shown in Figures 6.9 and 6.10.

The corresponding longitudinal acceleration responses are shown in Figures 6.11

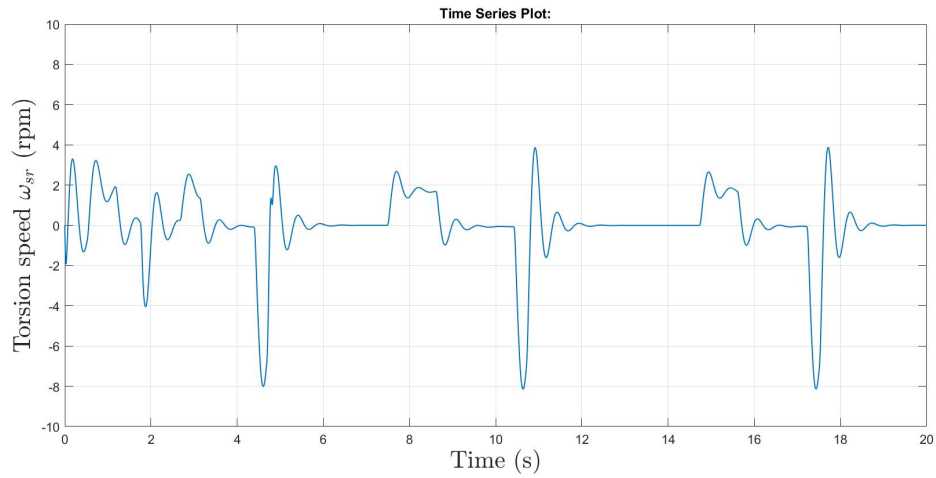


**Figure 6.3:** Torsion speed  $\omega_{sr}$  with 1st gear engaged and partial release of the accelerator.

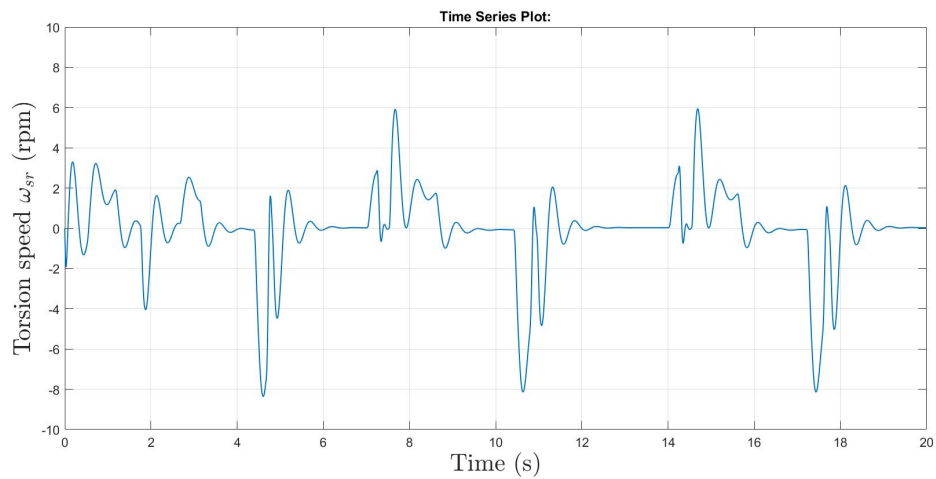


**Figure 6.4:** Torsion speed  $\omega_{sr}$  with 1st gear engaged and full release of the accelerator.

and 6.12. Note that, similar performance can also be obtained for higher gears with improvements in terms of attenuation of the longitudinal acceleration over time. For such reason, the design parameters collected in Table 6.1 for the third gear can be applied as the gear ratios decrease.

As it can be clearly seen, the performances obtained with the first gear engaged

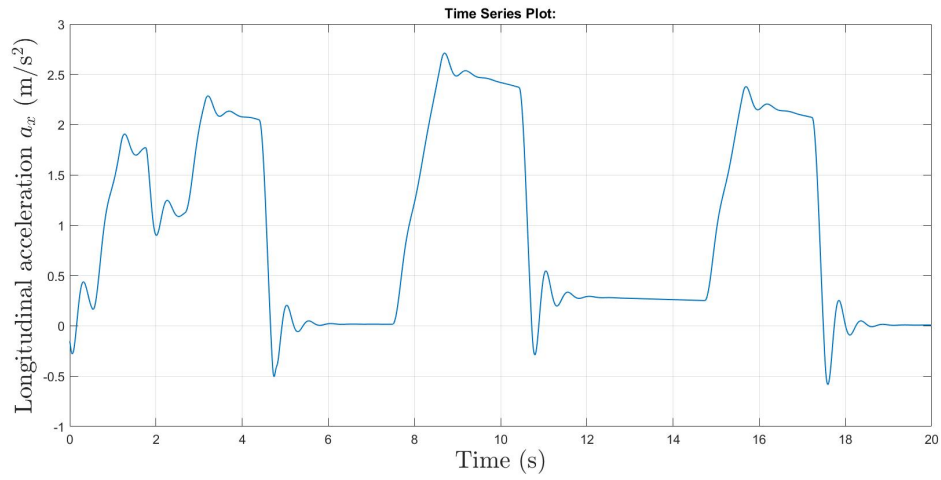


**Figure 6.5:** Longitudinal acceleration  $a_x$  with 1st gear engaged and partial release of the accelerator.

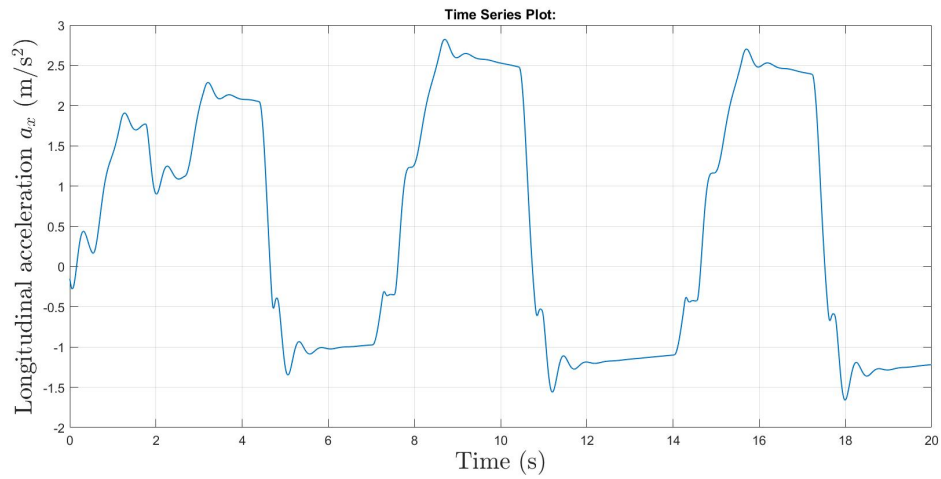


**Figure 6.6:** Longitudinal acceleration  $a_x$  with 1st gear engaged and full release of the accelerator.

is much worse with respect to those obtained for the third gear. Such difference is motivated by the high gear ratio  $\tau$  of the first gear, however, the use of a hybrid MPC controller shows a marked improvement in terms of attenuation of torsion oscillations with respect to transmissions in which a micro-slip controller is absent – i.e. whenever the torques generated by the engine are fully supplied to

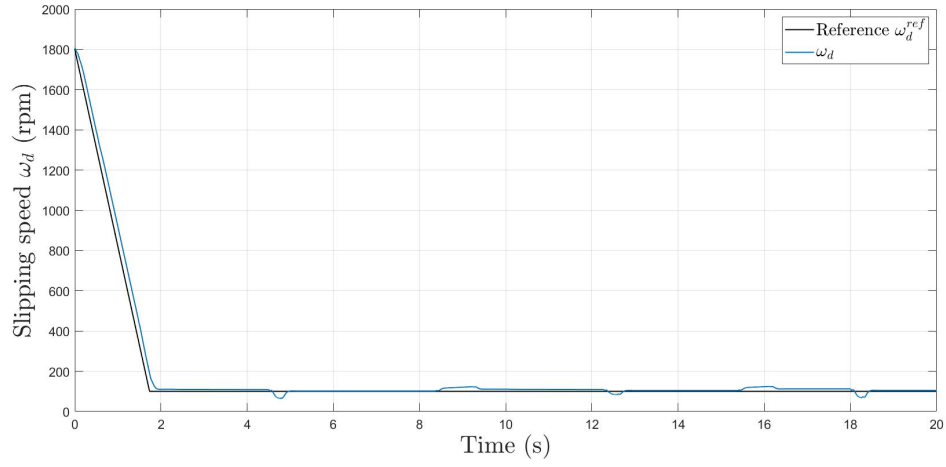


**Figure 6.7:** Slipping speed  $\omega_d$  with 3rd gear engaged and partial release of the accelerator.

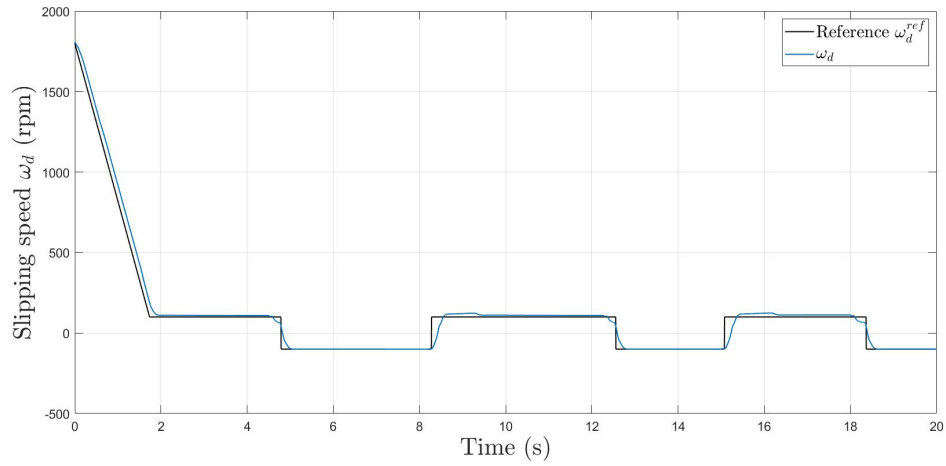


**Figure 6.8:** Slipping speed  $\omega_d$  with 3rd gear engaged and full release of the accelerator.

the transmission system. Figures 6.13 and 6.14 show what mentioned above for first and third gear respectively, considering full releases of the acceleration pedal.

An interesting observation regarding Figures 6.13 and 6.14 can be made. In fact, in both plots there are oscillations of the torsion speed controlled by the hybrid MPC which assumes counter-trend values with respect to those resulting from the

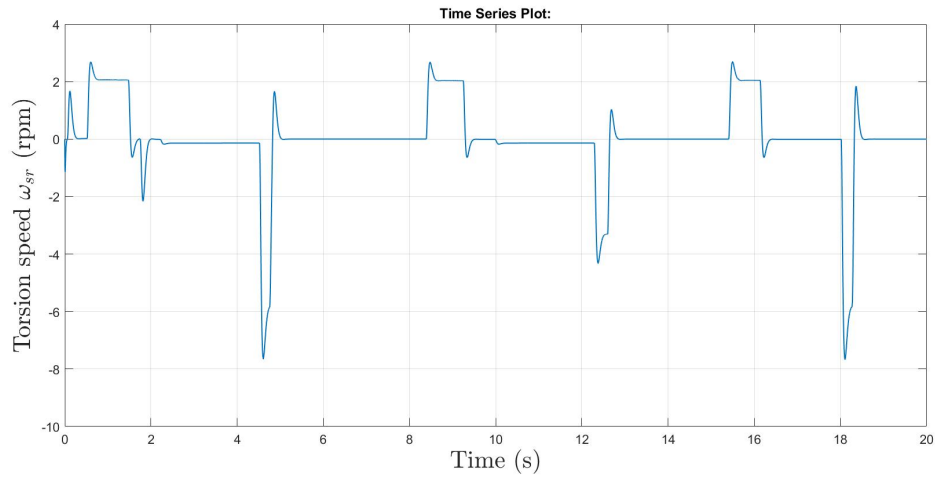


**Figure 6.9:** Torsion speed  $\omega_{sr}$  with 3rd gear engaged and partial release of the accelerator.

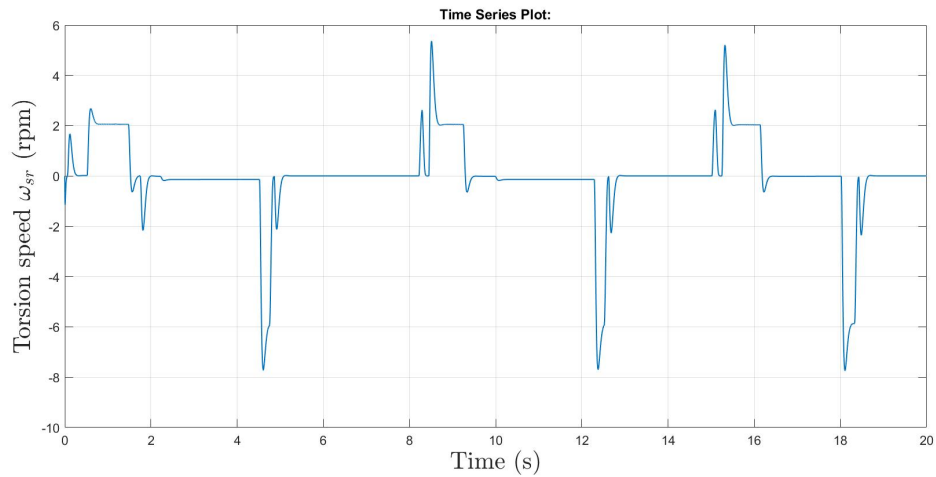


**Figure 6.10:** Torsion speed  $\omega_{sr}$  with 3rd gear engaged and full release of the accelerator.

absence of a control action. In particular, around 8.4 and 15.7 seconds of Figure 6.14 it can be seen how these oscillation peaks occur exactly in correspondence of the cut-off action imposed on the controller. It is therefore clear that the behavior of this action affects the control of the drive shaft oscillation dynamics by introducing an inevitable and not indifferent discontinuity.

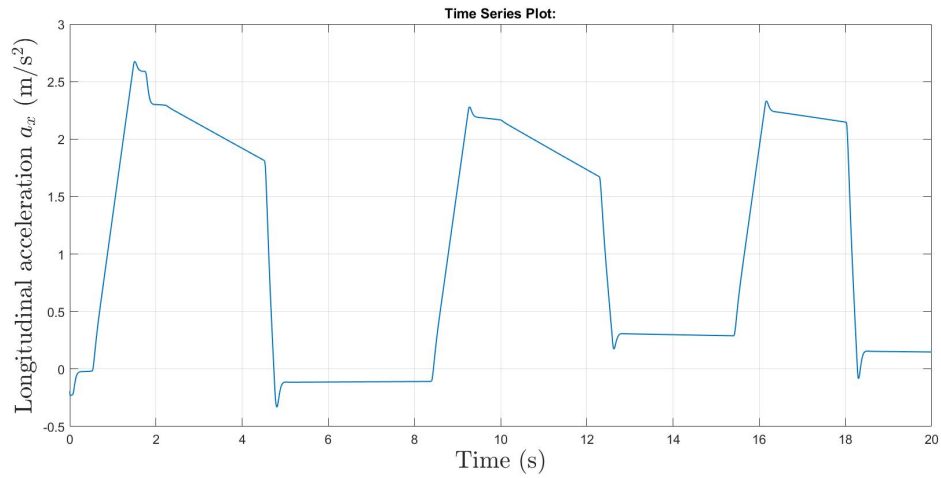


**Figure 6.11:** Longitudinal acceleration  $a_x$  with 3rd gear engaged and partial release of the accelerator.

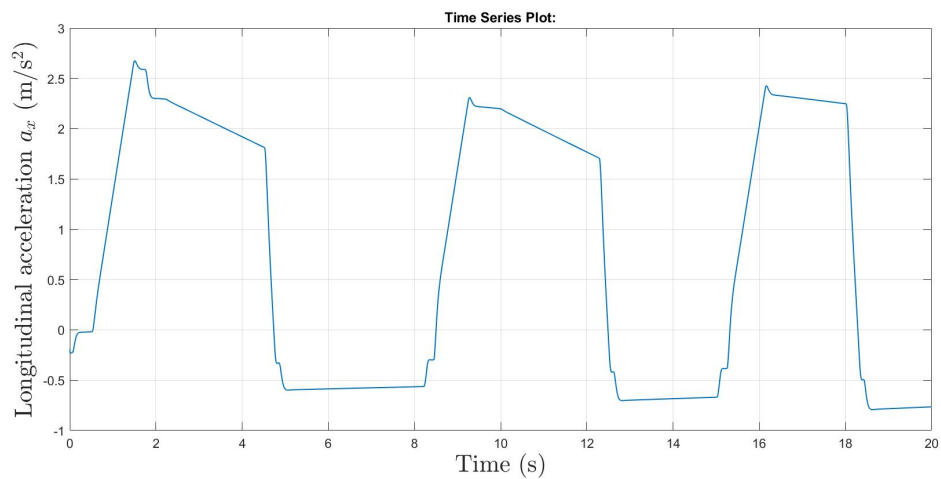


**Figure 6.12:** Longitudinal acceleration  $a_x$  with 3rd gear engaged and full release of the accelerator.

## 6.2 Tests with hybrid Kalman filter

In this section the hybrid Kalman filter introduced in section (5.5.4) is adopted in order to estimate quantities that are not available for measurements. Indeed, it often happens that such quantities are measured in place of simulation tests

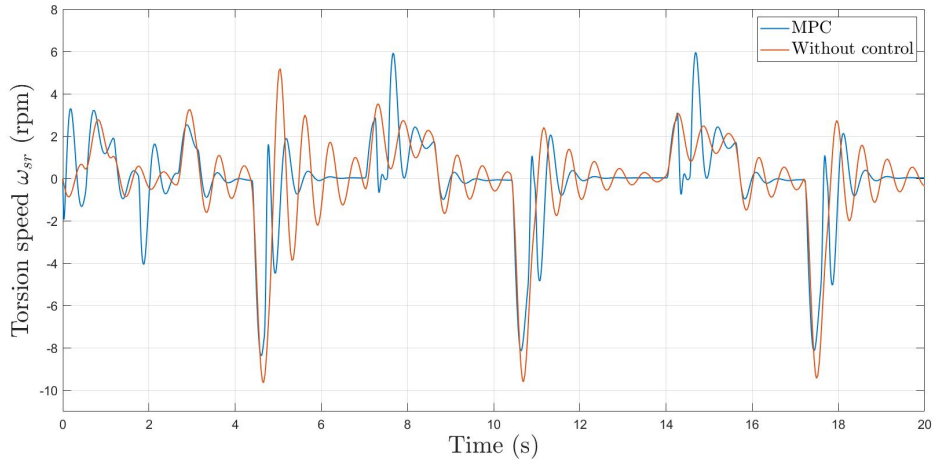


**Figure 6.13:** Torsion speed  $\omega_{sr}$  comparison with and without hybrid MPC controller. A full release of the accelerator and 1st gear engaged are considered.

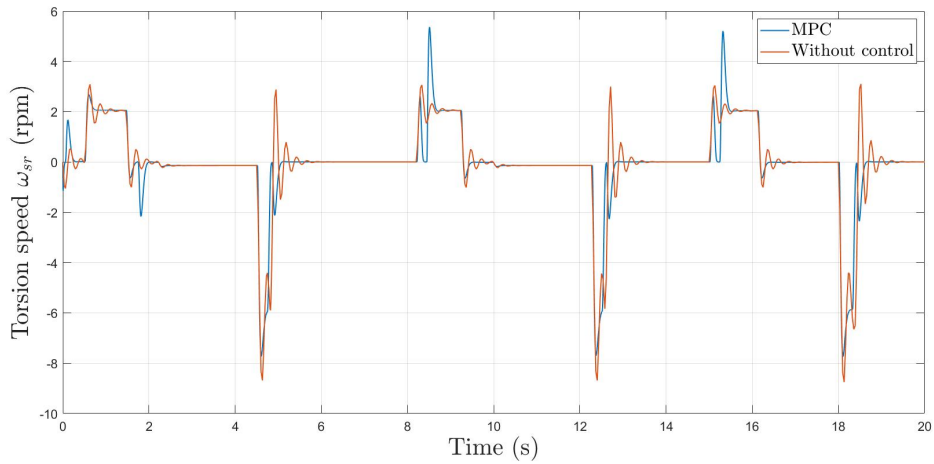


**Figure 6.14:** Torsion speed  $\omega_{sr}$  comparison with and without hybrid MPC controller. A full release of the accelerator and 3rd gear engaged are considered.

through suitable expensive industrial instruments (like the torque meter for the transmitted clutch torque) not used during normal driving. As in the calibration process of the hybrid MPC controller, several simulations are conducted in order to properly set the state observer. The tuning parameters of the former – i.e. the

entries of the matrices (5.34) are listed below:

$$\begin{aligned} q_{SO} &= 80000 \\ r_{SO} &= 0.1 \end{aligned} \tag{6.1}$$

Closed-loop simulations with estimated states feedback are performed in order to show the effectiveness of the Hybrid Kalman filter employed. In this regard, the following plots show the comparisons between the actual behaviors of the quantities under test and the estimated ones. Figures 6.15 , 6.16 and 6.17 show the estimations of the engine speed  $\omega_m$ , the primary shaft speed  $\omega_p$  and wheel speed  $\omega_r$  respectively with the first gear engaged.

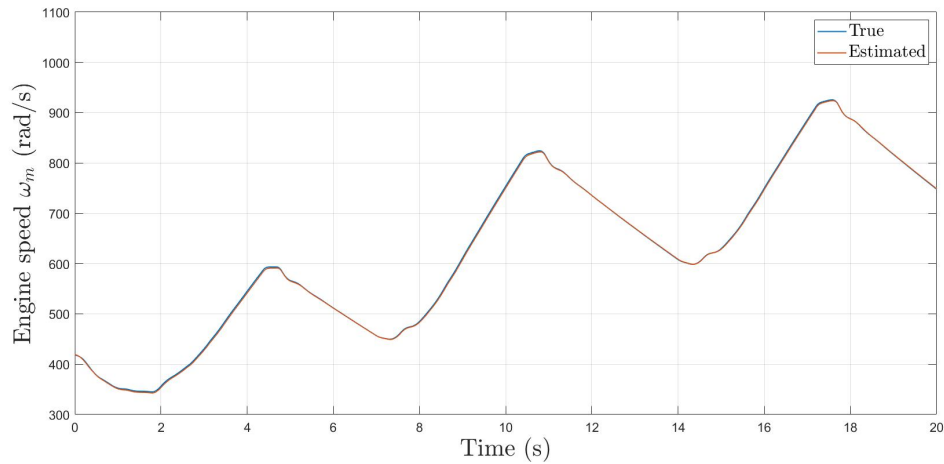


**Figure 6.15:** Engine speed  $\omega_m$  in 1st gear. Comparison between the true and the estimated quantity.

As it can be noticed, since these states are actually measurable, their estimate is faithful to their measure so that a filtering action can be applied. Similar results can be obtained with the third gear engaged as shown in Figures 6.18 , 6.19 and 6.20.

The estimation of the actually actuated clutch torque  $C_f$  and the torsional speed  $\omega_{sr}$  is quite challenging and it significantly depends on the choice of the Kalman SO parameters. In this context, the choice of a high value of the  $q_{SO}$  parameter allows an accurate estimation of  $C_f$  as depicted in Figure 6.21, on the contrary a slight difference between the actual and estimated  $\omega_{sr}$  can be seen in Figure 6.22 (1st gear).

The same reasoning holds for the maneuvers obtained in third gear as shown in Figures 6.23 and 6.24. In conclusion, despite some few minor differences, the

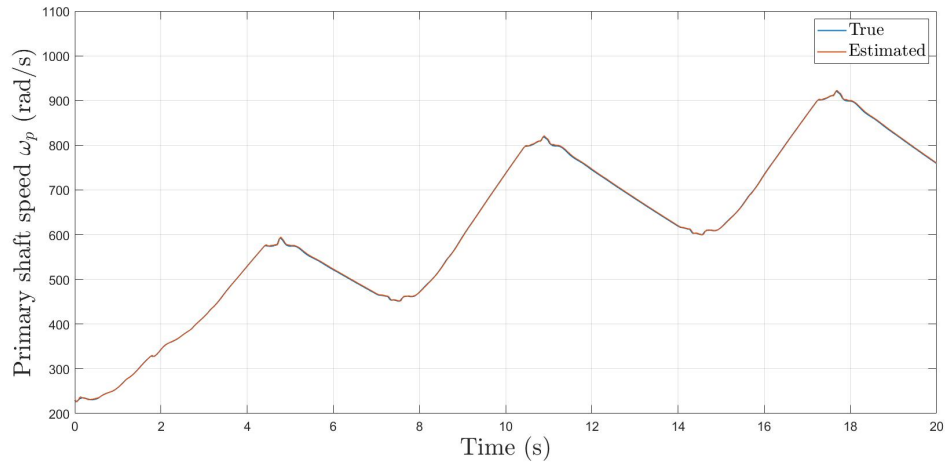


**Figure 6.16:** Primary shaft speed  $\omega_p$  in 1st gear. Comparison between the true and the estimated quantity.

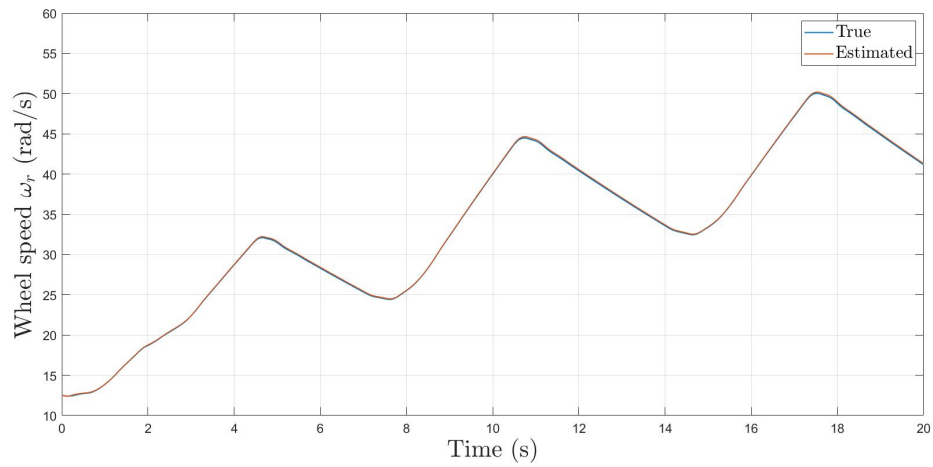


**Figure 6.17:** Wheel speed  $\omega_m$  in 1st gear. Comparison between the true and the estimated quantity.

inclusion of the hybrid Kalman SO does not significantly influence the system performance.

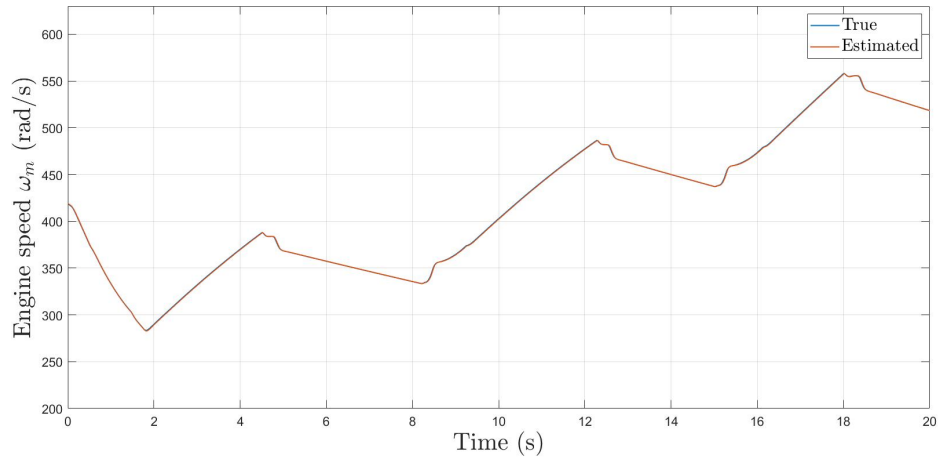


**Figure 6.18:** Engine speed  $\omega_m$  in 3rd gear. Comparison between the true and the estimated quantity.

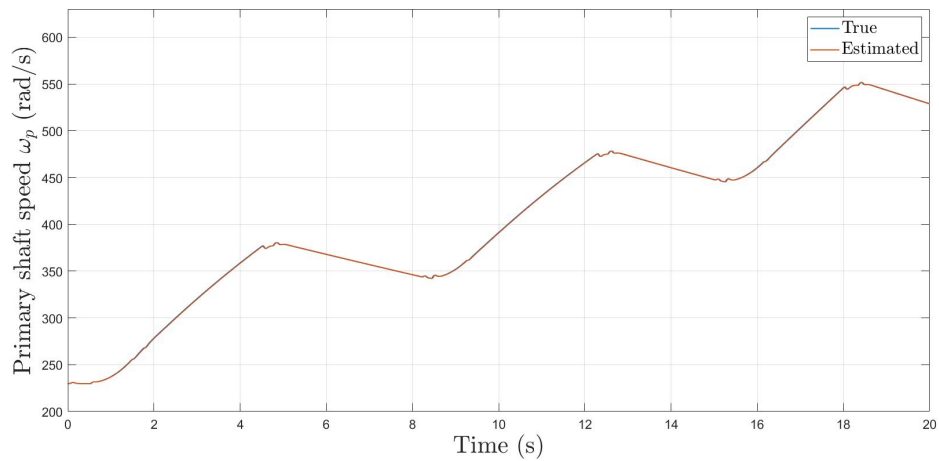


**Figure 6.19:** Primary shaft speed  $\omega_p$  in 3rd gear. Comparison between the true and the estimated quantity.

### 6.2.1 Transmissibility coefficient variation

An important aspect that must be taken into account concerns the variation of the transmissibility coefficient  $k_t$  introduced in section (3.2). In fact, the actuator is not always able to guarantee that the value of the actual transmitted torque  $C_f$  is equal to the one requested by the hybrid MPC controller. This happens due to

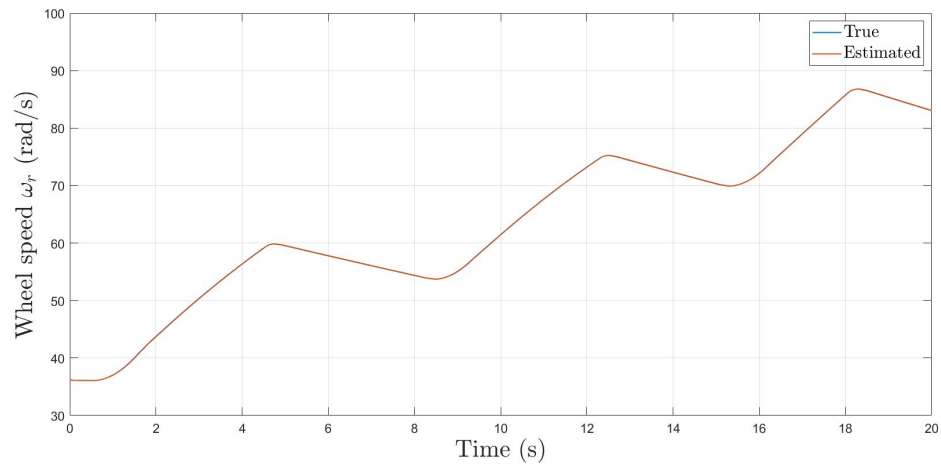


**Figure 6.20:** Wheel speed  $\omega_m$  in 3rd gear. Comparison between the true and the estimated quantity.

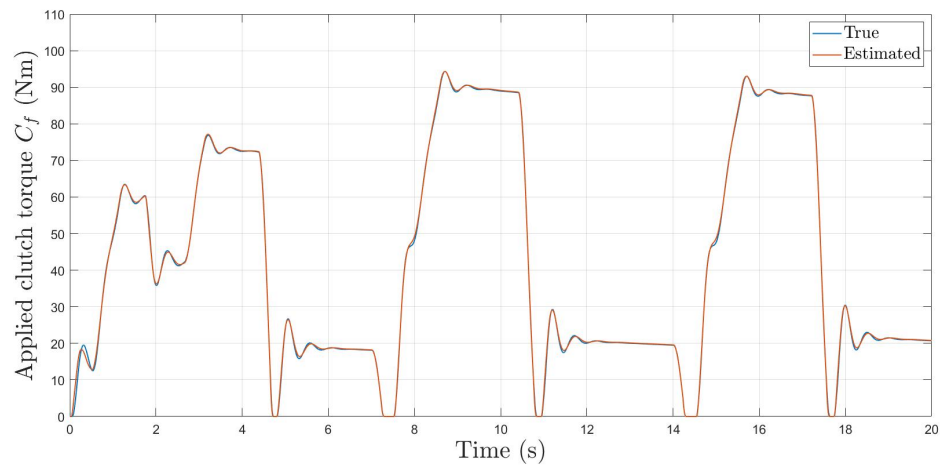


**Figure 6.21:** Actuated clutch torque  $C_f$  in 1st gear. Comparison between the true and the estimated quantity.

several reasons:

- the change in temperature of the clutch disks due to different working conditions;
- the wear of the clutch;

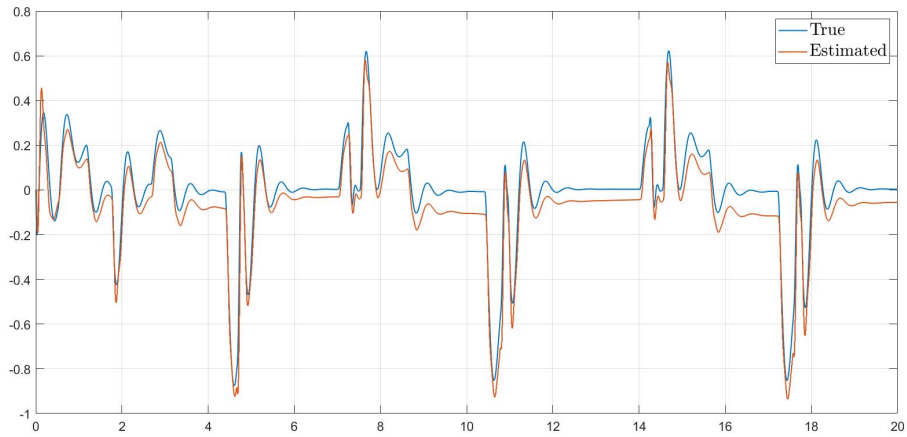


**Figure 6.22:** Torsion speed  $\omega_{sr}$  in 1st gear. Comparison between the true and the estimated quantity.

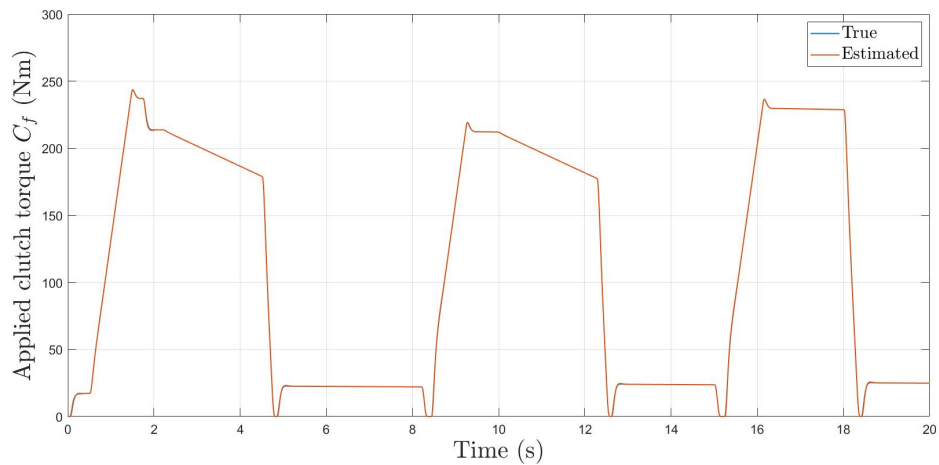


**Figure 6.23:** Actuated clutch torque  $C_f$  in 3rd gear. Comparison between the true and the estimated quantity.

- the difference in the driving style that can affect the mechanical properties of the clutch.

As a first approximation, all the factors mentioned above are included inside the  $k_t$  coefficient and a 10% variation from its nominal value is considered:

$$0.9 \leq k_t \leq 1.1 \quad (6.2)$$

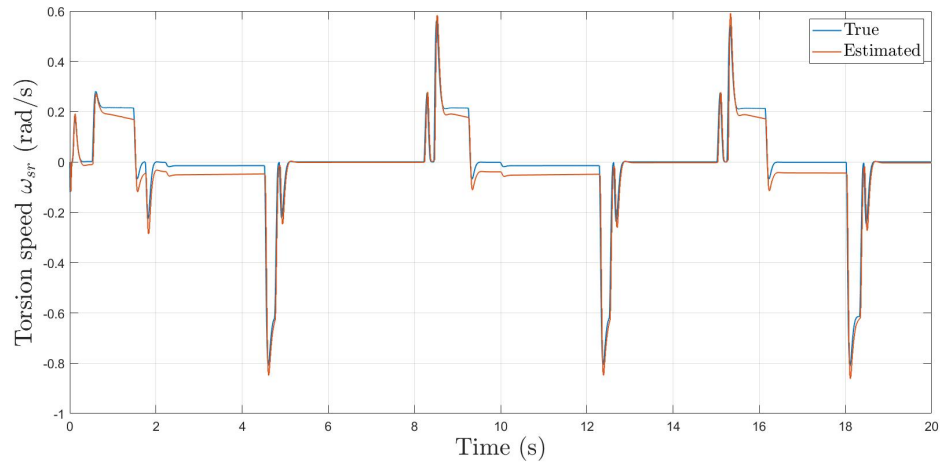


**Figure 6.24:** Torsion speed  $\omega_{sr}$  in 3rd gear. Comparison between the true and the estimated quantity.

As far as the slipping speed tracking is concerned, Figures 6.25 and 6.26 report the effects of the the gain  $Kt$  variation for first and third gear respectively, while Figures 6.27 and 6.28 show the same analysis on the torsion speed  $\omega_{sr}$ .

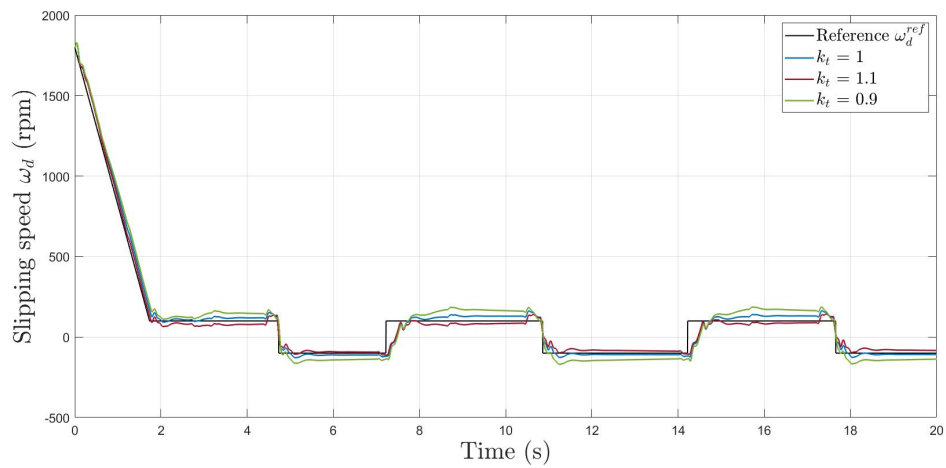


**Figure 6.25:** Slipping speed for different values of the transmissibility gain  $K_t$  on 1st gear.

The variation of the transmissibility coefficient leads to a general degradation of the performances in terms of  $\omega_d$  tracking and attenuation of torsional oscillations.

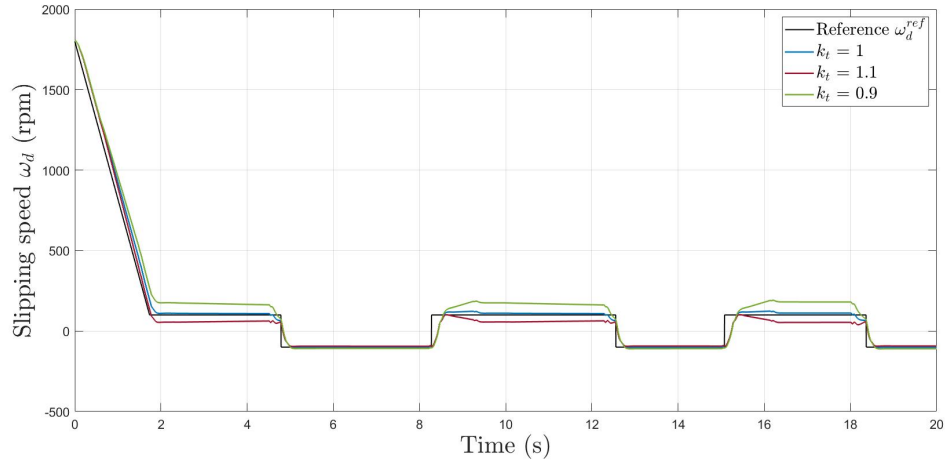


**Figure 6.26:** Slipping speed for different values of the transmissibility gain  $K_t$  on 3rd gear.

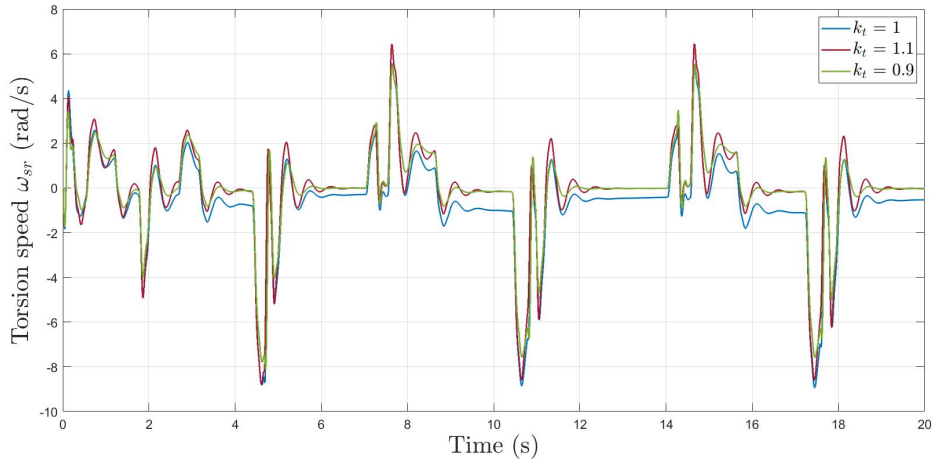


**Figure 6.27:** Torsion speed for different values of the transmissibility gain  $K_t$  on 1st gear.

Specifically, a 10% less variation with respect to the nominal condition ( $k_t = 1$ ) has a strong negative effect on the tracking performance. On the contrary, the worst control performance for the torsion speed is obtained with  $K_t = 1.1$ .

An important consideration concerns the effects of the gain  $k_t$  on the requested and applied clutch torque. Figures 6.29 and 6.30 show how the hybrid MPC

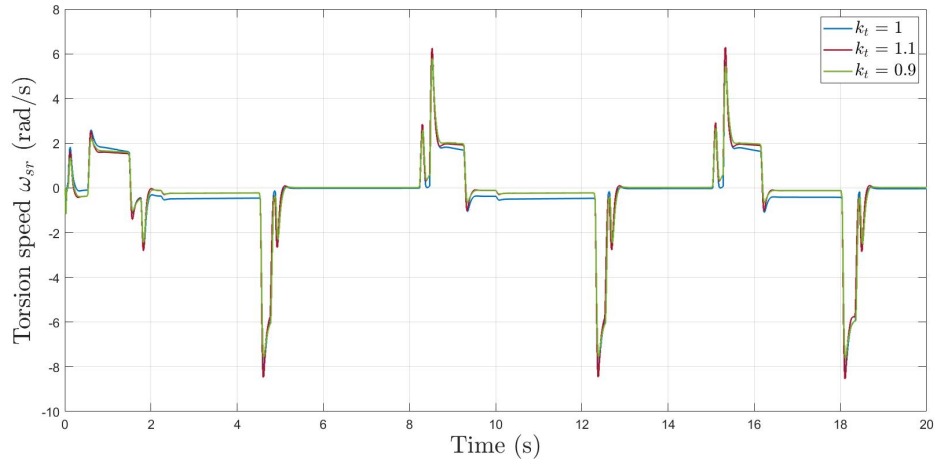


**Figure 6.28:** Torsion speed for different values of the transmissibility gain  $K_t$  on 3rd gear.

controller is able to compensate the effect of the transmissibility coefficient variations acting on the requested torque  $C_f^{req}$ . In particular, in the case of  $K_t = 0.9$  the requested torque is higher than the nominal one, while for  $K_t = 1.1$ , being the actually applied torque  $C_f$  higher, the control input  $C_f^{req}$  is lower. This behavior is due to the MPC intrinsic robustness properties that allow, except for transients, the transmitted torque  $C_f$  to be very close to the nominal values. Figures 6.31 and 6.32 show similar results for third gear where, thanks to the lower gear ratio, the resulting control action is more accurate and effective.

### 6.3 Observations

As a result of the previous simulations, multiple observations can be outlined.

1. On one hand, the use of an hybrid MPC controller allows an effective management of the sign inversion of the slipping speed together with all the advantages of a classic Model Predictive Control strategy. On the other hand, the hybrid formulation suffers in terms of modeling complexity and computational speed. In this context, a good strategy could be to simplify the model dynamics and decrease the prediction horizon appropriately.
2. The attenuation of torsional oscillations as well as slipping speed reference tracking is quite challenging whenever the first gear is engaged. Further

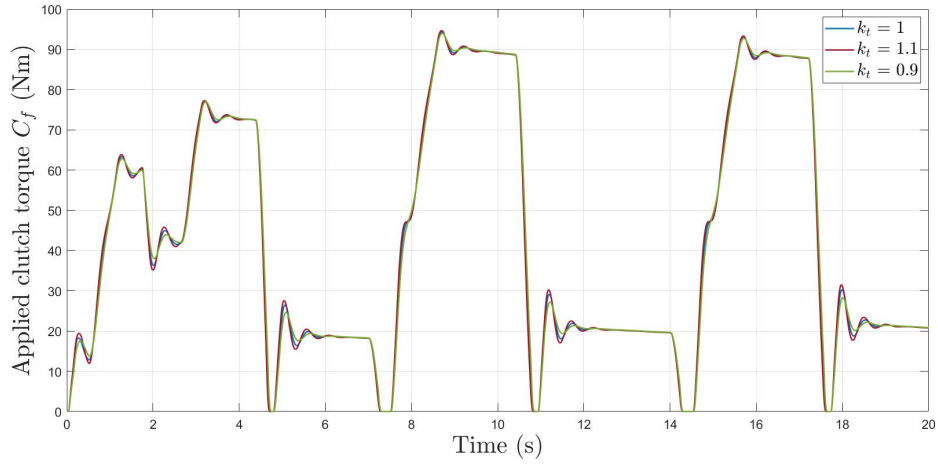


**Figure 6.29:** Applied torque  $Cf$  for different values of the transmissibility gain  $K_t$  (1st gear).

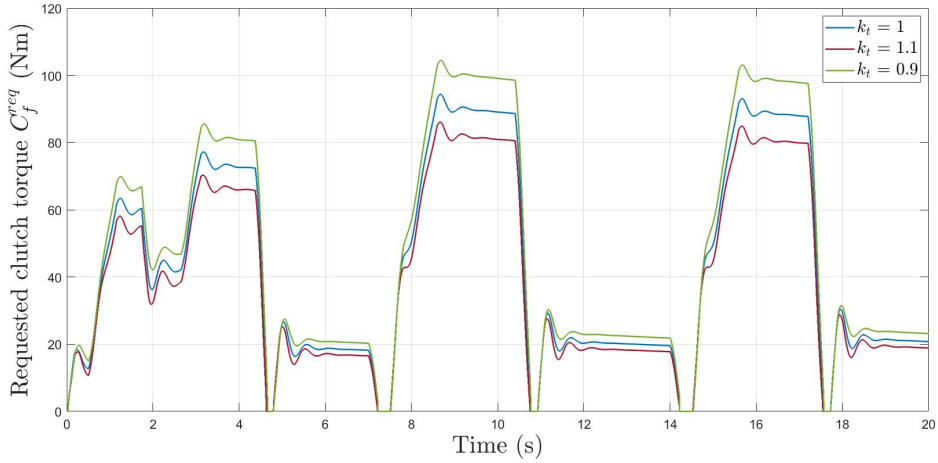


**Figure 6.30:** Requested clutch torque  $Cf$  for different values of the transmissibility gain  $K_t$  (1st gear).

improvements can be obtained with a better tuning of the hybrid MPC parameters.

3. The presence of the cut-off logic introduced to avoid bang-bang behaviors inside the control input signal leads to temporary oscillations which results in high value peaks of the torsion oscillation  $\omega_{sr}$ . This kind of problem is a side

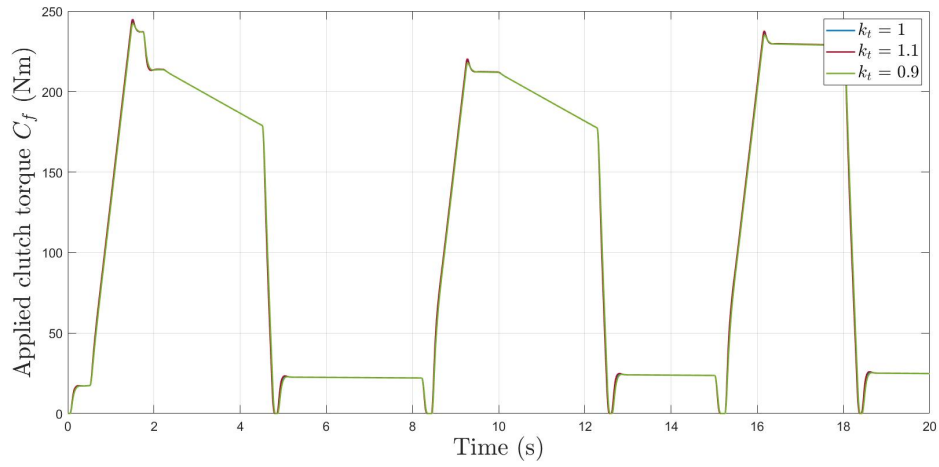


**Figure 6.31:** Applied torque  $Cf$  for different values of the transmissibility gain  $K_t$  (3rd gear).

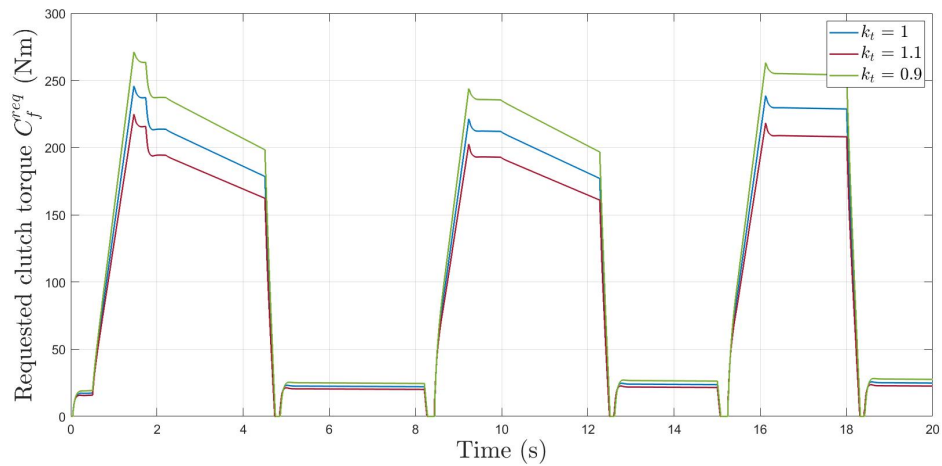


**Figure 6.32:** Requested clutch torque  $Cf$  for different values of the transmissibility gain  $K_t$  (3rd gear).

effect resulting from the nature of the control strategy adopted and cannot be avoided.

4. The variation of the actuator transmissibility factor is critical. Indeed, although the hybrid MPC controller tries to compensate  $k_t$  variations, the values of the transmitted torque tend to deviate from their nominal condition, especially

during transients. This issue affects both the inaccurate reference tracking and the poor attenuation of the driveline oscillations. A possible solution could be to use the hybrid Kalman SO whose estimations partially overcome the problem.

5. The use of the Kalman filter is encouraged in the perspective of including constraints on the actuated clutch torque (instead of the requested clutch torque), especially whenever variations on the transmissibility coefficient occur. Clearly this choice limits the feasibility of the optimal solutions computed by the controller.

## Chapter 7

# Conclusions

In the present dissertation, a novel Hybrid micro-slip MPC control for automated manual transmission system has been studied with the aim of improving the driving experience by attenuating the fluctuations inside the driveline and managing the problem of the sign inversion of the clutch slipping speed by controlling the transmitted torque. In particular, the proposed approach has gone through the development of a Piecewise Affine system useful in describing the non-linear dynamic of the considered transmission and the formulation of a suitable Mixed-Integer Quadratic Programming problem.

The tracking of a reference slipping speed together with the minimization of the driveline torsional oscillations have been carried out through simulations performed on both first and third gear. The adopted control architecture shows its effectiveness with respect to the absence of control on the transmitted clutch torque.

A brief sensitivity analysis has proven that, although the effects of uncertainties have not been explicitly taken into account from the design procedure, the hybrid MPC approach is able to achieve quite good performances in the presence of different operating conditions. In this context, a significant improvement in terms of attenuation of vibrations and reference tracking has been introduced thanks to the inclusion of a hybrid Kalman state observer used for the estimation of non-measurable variables such as the applied clutch torque and torsion speed of the transmission shaft.

## 7.1 Future works

Starting from the results presented in this thesis project, further studies can be conducted in order to improve the overall performances of the considered control architecture. Examples of possible new solutions concern:

- the development of a three-regions PWA system with the inclusion of Boolean state variables describing the logic behind the change of the working regions. With this solution the binary states can be included inside the cost function so that the hybrid MPC controller can predict whether a change of operating condition occurs during the prediction.
- The inclusion of robust techniques for hybrid MPC controllers ensuring recursive feasibility.
- Investigations about the use of the engine torque as a further control input variable in order to improve the transmission system performances.

# Bibliography

- [1] W Reik, A Albers, M Schnurr, et al. «Torque Control Isolation (TCI) The Smart Clutch». In: LuK-Symposium. 1990 (cit. on p. 15).
- [2] T. Jin, P. Li, and G. Zhu. «Optimal decoupled control for dry clutch engagement». In: *2013 American Control Conference*. 2013, pp. 6740–6745. DOI: 10.1109/ACC.2013.6580898 (cit. on pp. 15, 16).
- [3] L. Glielmo, L. Iannelli, V. Vacca, and F. Vasca. «Gearshift control for automated manual transmissions». In: *IEEE/ASME Transactions on Mechatronics* 11.1 (2006), pp. 17–26. DOI: 10.1109/TMECH.2005.863369 (cit. on pp. 15, 16).
- [4] Franco Garofalo, Luigi Glielmo, Luigi Iannelli, and Francesco Vasca. «OPTIMAL TRACKING FOR AUTOMOTIVE DRY CLUTCH ENGAGEMENT». In: *IFAC Proceedings Volumes* 35.1 (2002). 15th IFAC World Congress, pp. 367–372. ISSN: 1474-6670. DOI: <https://doi.org/10.3182/20020721-6-ES-1901.01529>. URL: <https://www.sciencedirect.com/science/article/pii/S147466701539950X> (cit. on p. 16).
- [5] A. Bemporad, F. Borrelli, L. Glielmo, and F. Vasca. «Hybrid control of dry clutch engagement». In: *2001 European Control Conference (ECC)*. 2001, pp. 635–639. DOI: 10.23919/ECC.2001.7075980 (cit. on p. 16).
- [6] Pietro J Dolcini, Carlos Canudas-de-Wit, and Hubert Béchart. *Dry clutch control for automotive applications*. Springer Science & Business Media, 2010 (cit. on pp. 16, 17).
- [7] Simone Baliva. *Micro-slip control of a Dry Dual Clutch Transmission system using Model Predictive Control techniques*. XXX, 2015 (cit. on pp. 17–19).
- [8] Andreas Myklebust. «Dry clutch modeling, estimation, and control». PhD thesis. Linköping University Electronic Press, 2014 (cit. on p. 18).
- [9] Francesco Borrelli, Alberto Bemporad, and Manfred Morari. *Predictive Control for Linear and Hybrid Systems*. Cambridge University Press, 2017. DOI: 10.1017/9781139061759 (cit. on pp. 21, 22).

- [10] Domenico Mignone. «Control and estimation of hybrid systems with mathematical optimization». PhD thesis. ETH Zurich, 2002 (cit. on p. 24).
- [11] Alberto Bemporad, Giancarlo Ferrari-Trecate, and Manfred Morari. «Observability and controllability of piecewise affine and hybrid systems». In: *IEEE transactions on automatic control* 45.10 (2000), pp. 1864–1876 (cit. on p. 24).
- [12] Domenico Mignone, Alberto Bemporad, and Manfred Morari. «A framework for control, fault detection, state estimation, and verification of hybrid systems». In: *Proceedings of the 1999 American Control Conference (Cat. No. 99CH36251)*. Vol. 1. IEEE. 1999, pp. 134–138 (cit. on p. 24).
- [13] F. D. Torrisi and A. Bemporad. «HYSDEL—a tool for generating computational hybrid models for analysis and synthesis problems». In: *IEEE Transactions on Control Systems Technology* 12.2 (2004), pp. 235–249. DOI: 10.1109/TCST.2004.824309 (cit. on p. 25).
- [14] JB Rawlings and DQ Mayne. «Postface to model predictive control: Theory and design». In: *Nob Hill Pub* 5 (2012), pp. 155–158 (cit. on p. 28, 32).
- [15] Alberto Bemporad, Manfred Morari, Vivek Dua, and Efstratios N Pistikopoulos. «The explicit linear quadratic regulator for constrained systems». In: *Automatica* 38.1 (2002), pp. 3–20 (cit. on p. 29).
- [16] Stephen Boyd, Stephen P Boyd, and Lieven Vandenbergh. *Convex optimization*. Cambridge university press, 2004 (cit. on p. 29).
- [17] Hans Mittelmann. *BENCHMARKS FOR OPTIMIZATION SOFTWARE*. 2019. URL: <http://plato.la.asu.edu/bench.html> (visited on 03/22/2021) (cit. on p. 31).
- [18] LLC Gurobi Optimization. *Gurobi Optimizer Reference Manual*. 2021. URL: <http://www.gurobi.com> (cit. on p. 31).
- [19] L. Magni and R. Scattolini. *Complementi di controlli automatici*. Pitagora, 2006 (cit. on p. 46).
- [20] A. Bemporad. *Hybrid Toolbox - User's Guide*. <http://cse.lab.imtlucca.it/~bemporad/hybrid/toolbox>. 2004 (cit. on p. 49).
- [21] M. Kvasnica, P. Grieder, and M. Baotić. *Multi-Parametric Toolbox (MPT)*. 2004. URL: <http://control.ee.ethz.ch/~mpt/> (cit. on p. 49).